Copula-Probabilistic Flood Risk Analysis with an Hourly Flood Monitoring Index

Ravinesh Chand [1], Thong Nguyen-Huy [2,3,*], Ravinesh C. Deo [1], Sujan Ghimire [1], Mumtaz Ali [4,5] and Afshin Ghahramani [6,†]

[1] School of Mathematics, Physics and Computing, University of Southern Queensland, Springfield, QLD 4300, Australia; u1151334@umail.usq.edu.au (R.C.); ravinesh.deo@unisq.edu.au (R.C.D.); sujan.ghimire@unisq.edu.au (S.G.)

[2] Centre for Applied Climate Sciences, University of Southern Queensland, Toowoomba, QLD 4350, Australia

[3] Faculty of Information Technology, Thanh Do University, Kim Chung, Hoai Duc, Ha Noi 100000, Vietnam

[4] UniSQ College, University of Southern Queensland, Toowoomba, QLD 4350, Australia; mumtaz.ali@unisq.edu.au

[5] New Era and Development in Civil Engineering Research Group, Scientific Research Center, Al-Ayen University, Thi-Qar, Nasiriyah 64001, Iraq

[6] University of Southern Queensland, Toowoomba, QLD 4350, Australia; afshin.ghahramani@des.qld.gov.au

[*] Correspondence: thong.nguyen-huy@unisq.edu.au or nhthong@thanhdouni.edu.vn

[†] Current address: Department of Environment and Science and Innovation, Queensland Government, Toowoomba, QLD 4350, Australia.

Abstract: Floods are a common natural disaster whose severity in terms of duration, water resource volume, peak, and accumulated rainfall-based damage is likely to differ significantly for different geographical regions. In this paper, we first propose a novel hourly flood index ($SWRI_{24-hr-S}$) derived from normalising the existing 24-hourly water resources index ($WRI_{24-hr-S}$) in the literature to monitor flood risk on an hourly scale. The proposed $SWRI_{24-hr-S}$ is adopted to identify a flood situation and derive its characteristics, such as the duration (D), volume (V), and peak (Q). The comprehensive result analysis establishes the practical utility of $SWRI_{24-hr-S}$ in identifying flood situations at seven study sites in Fiji between 2014 and 2018 and deriving their characteristics (i.e., D, V, and Q). Secondly, this study develops a vine copula-probabilistic risk analysis system that models the joint distribution of flood characteristics (i.e., D, V, and Q) to extract their joint exceedance probability for the seven study sites in Fiji, enabling probabilistic flood risk assessment. The vine copula approach, particularly suited to Fiji's study sites, introduces a novel probabilistic framework for flood risk assessment. The results show moderate differences in the spatial patterns of joint exceedance probability of flood characteristics in different combination scenarios generated by the proposed vine copula approach. In the worst-case scenario, the probability of any flood event occurring where the flood volume, peak, and duration are likely to exceed the 95th-quantile value (representing an extreme flood event) is found to be less than 5% for all study sites. The proposed hourly flood index and the vine copula approach can be feasible and cost-effective tools for flood risk monitoring and assessment. The methodologies proposed in this study can be applied to other data-scarce regions where only rainfall data are available, offering crucial information for flood risk monitoring and assessment and for the development of effective mitigation strategies.

Keywords: flood characteristics; flood monitoring; hourly flood index; joint distribution; risk mitigation; vine copulas

1. Introduction

Flooding is a catastrophic natural disaster progressively increasing in frequency and severity, primarily attributed to climate change–induced phenomena such as increased rainfall intensity. Generally, there are three prevalent flood types: fluvial or river floods,

pluvial or flash floods, and coastal floods [1,2]. A flash flood is a sudden and severe local inundation often resulting from high-intensity rainfall (e.g., tropical cyclones, slow-moving tropical depressions, or thunderstorms) within a short period (usually less than six hours) and/or may also be caused by sudden discharge of impounded water (e.g., dam or levee failures, ice jam release, or a glacier lake outburst) [3,4]. Flash floods can affect a range of locations, including river plains, valleys, and areas with steep terrain, elevated surface runoff rates, constrained stream channels, and persistent heavy convective rainfall [3]. They often necessitate prompt action to mitigate their severe impact, typically relying on expeditious decision-making and emergency response. Flash floods make up about 85% of all floods, resulting in more than 5000 deaths annually and causing severe social, economic, and environmental impacts [5]. The repercussions of flood disasters are more devastating in developing countries such as Fiji [6], where this study is focused. Therefore, developing a real-time flood risk monitoring tool remains an ongoing research motivation to enable an assessment of flood occurrences for early warning systems in Fiji.

Fiji experiences regular flooding events arising from orographic rainfall due to the topography of its larger islands, including Viti Levu and Vanua Levu, which have a maximum elevation of 1300 m above sea level, along with the impact of prevailing southeast trade winds [7]. For Fiji, about 90% of its population resides in coastal areas susceptible to floods [8]. Between 1970 and 2016, Fiji faced 44 major flood events, impacting approximately 563,310 people and resulting in 103 fatalities [9]. The most catastrophic floods occurred in 2004, 2009, 2012 (including the January and March flood events), and 2014. The 2009 and 2012 events, considered among the worst in the nation's history, resulted in over 200 million FJD in damages and losses, causing 15 fatalities and directly affecting more than 160,000 people [9]. For Fiji, the estimated average annual flood losses exceed 400 million FJD, equivalent to 4.2% of Fiji's Gross Domestic Product (GDP) [9]. These are substantial losses for a small island nation with a population of less than a million and a GDP of less than 5 billion USD [10]. Under the assumption that climate change conditions will significantly increase rainfall, the annual flood-related asset losses could exceed 5% of Fiji's GDP by 2050 without adaptation measures [9]. As a result, it is imperative to develop reliable methods for accurately monitoring flood risk on near real-time (e.g., hourly) timescales to mitigate the severe impacts of flooding.

Intense and/or prolonged precipitation is among the primary causes of floods. However, to better understand flood risk, multiple factors must be considered. These include the combined impact of various weather or climate events such as temperature and precipitation (while these events may not individually reach extreme levels, their cumulative effect can result in severe impacts) as well as the vulnerability and exposure of the affected area [11,12]. Climate change also induces changes in various flood-related factors, including precipitation, soil moisture content, sea level, and glacial lake conditions, potentially changing flood characteristics [12]. Other factors, such as land use and cover, catchment size and shape, drainage networks, and dam or levee construction, can also influence flood dynamics. Hence, an index that integrates all these factors and the accumulative impacts of other weather or climate characteristics is essential for a comprehensive flood risk assessment.

In many developing nations where flood monitoring resources, hydro-meteorological datasets, and risk monitoring facilities are underdeveloped, applying a mathematically derived flood index utilising only rainfall data provides a key strategy for assessing an impending flood risk situation. Some of the key mathematical indices used previously in flood risk monitoring include the Standardised Precipitation Index (SPI), the Available Water Resources Index ($AWRI$), the Weighted Average of Precipitation (WAP), the Standardised WAP ($SWAP$), the Flood Index (I_F), and the Standardised Antecedent Precipitation Index ($SAPI$) [13–18]. The flood indices, such as $AWRI$, $SWAP$, I_F, and $SAPI$, are robust as they are designed to account for changes in antecedent or immediate past rainfall by employing a suitable time-dependent reduction function that accounts for the depletion of water resources through various hydrological processes. For example, the daily flood index, I_F,

applied in Australia [17,19,20], Iran [21], Bangladesh [22,23], and Fiji [6], has shown good performance in monitoring flood events on a daily scale. Despite its benefits, one primary weakness of I_F and other indices, such as SPI, lies in their utilisation of daily, monthly, or annual accumulated rainfall data, which represent much longer timescales than what is required in a flash flood monitoring system. Consequently, these indices fail to adequately represent the flood risk caused by bursts of high-intensity rainfall and rapid responses leading to flash flood events.

The present study draws relevance from a pilot study conducted by Deo et al. [24] that proposed a 24-h water resources index ($WRI_{24-hr-S}$) based on a concept similar to the $AWRI$, which was applied in two study locations, Australia and South Korea, to monitor the flash flood risk in sustained extreme rainfall periods. The $WRI_{24-hr-S}$ monitors flood risk by considering the contribution of accumulated rainfall in the past 24 h, whereby the rainfall contribution from the preceding hours is subjected to the time-dependent reduction function that accounts for the depletion of water resources through various hydrological processes such as evaporation, percolation, seepage, runoff, and drainage. However, unlike $SAPI$ and I_F, which are normalised values derived from the Antecedent Precipitation Index (API) and the $AWRI$, respectively, the identification of flood events and the computation of their characteristics are not achievable with the current form of $WRI_{24-hr-S}$. This is primarily because this index is unnormalised and does not enable objective assessment of flood risk across geographically diverse study sites.

To enhance the understanding of flood risks, it is essential to calculate the flood characteristics, including the volume (V), peak (Q), and duration (D) that concurrently result in major collateral damage. As the flood characteristics such as the D, V, and Q are mostly interrelated, we envisage that these characteristics should be jointly considered in a multivariate analysis model to estimate the actual probability of a flood occurrence [18,25]. Importantly, any model representing the joint distribution of D, V, Q, and other crucial flood characteristics, such as the onset and withdrawal of a flood event, can provide significant insights into the relative severity of any flood event. After the initial study of Sklar [26], copula-based models became attractive in modelling interrelated variables, albeit using a multivariate approach. As such, copulas can jointly model the distribution of flood characteristics such as the D, V, and Q, regardless of their marginal distributions or whether their dependence structure is linear or non-linear [18]. Vine copulas have recently shown superior capabilities in modelling flood characteristics compared to traditional Archimedean and elliptical copulas [18,27–29]. Therefore, this research follows a recent study by Nguyen-Huy et al. [18], which used vine copulas to model the joint distribution of extreme flood characteristics derived using the $SAPI$ in Myanmar. Their study has provided interesting insights into the probabilistic flood risk analysis. To the best of our knowledge, no prior research has applied vine copulas to analyse the probabilistic flood risk in Fiji despite floods being a catastrophic phenomenon on this small island nation.

The scientific contributions of this paper, with significant implications for flood risk monitoring and assessment, are threefold. Firstly, the paper advances the concept of the 24 h water resources index pioneered by Deo et al. [24] and formulates a novel hourly flood index ($SWRI_{24-hr-S}$) (a normalised metric) by normalising the 24-hourly water resources index in such a way that enables the objective assessment of flood risk across geographically diverse study sites. Secondly, the present study adopts the $SWRI_{24-hr-S}$, which is computed using real-time hourly rainfall data from 2014 to 2018 obtained from the Fiji Meteorological Services (FMS), to evaluate its practical utility in identifying flood situations and computing their associated flood characteristics (i.e., D, V, and Q) for seven different study sites in Fiji. Thirdly, the present study develops the vine copula approach for the first time to model the joint distribution of D, V, and Q derived from the $SWRI_{24-hr-S}$ for specific cases of Fiji's flood events to extract their joint exceedance probabilities for probabilistic flood risk assessment. Fiji is a Pacific Small Island Developing State (PSIDS) that frequently experiences recurrent flooding. The lack of advanced infrastructure and necessary data in Fiji makes continuous flood risk monitoring and assessment challenging.

The main aim of the present study is, therefore, to develop a novel hourly flood index, $SWRI_{24-hr-S}$, using only hourly rainfall data (which are readily available for the present study sites) and to conduct a probabilistic flood risk assessment by modelling the joint distribution of extreme flood characteristics derived from the $SWRI_{24-hr-S}$ for Fiji's case studies. Hence, the methodologies presented in this study aim to enhance and contribute to existing monitoring and early warning systems for flash floods in Fiji. Moreover, these approaches may also be applied in other flood-prone regions globally, particularly those facing similar data scarcity challenges. By adapting these methodologies, vulnerable communities can benefit from improved flood preparedness and mitigation strategies.

The rest of the paper is structured as follows. Section 2 provides information on the study area, the dataset used, and data pre-processing steps. It also encompasses the mathematical methodology for computing the hourly flood index and the flood characteristics. Additionally, it provides details on Vine copula models and equations used for computing the joint exceedance probability of flood characteristics. Section 3 provides the results and discussion. Section 4 highlights the key findings, the study's limitations, and insights for future research.

2. Materials and Methods

2.1. Study Area

The proposed copula-probabilistic flood risk analysis system based on the hourly flood index was applied to geographically diverse sites in Fiji. Fiji is located in the South Pacific Ocean at a latitude of 15° S to 22° S and a longitude of 177° W to 174° E (Figure 1), with a tropical maritime climate characterised by warm temperatures throughout the year [30,31]. The nation comprises an archipelago of 332 islands, 111 of which are permanently inhabited, with a total land area of about 18,333 km^2 [30]. Viti Levu (10,400 km^2) and Vanua Levu (5540 km^2) are two large mountainous islands covering about 87% of the total land area [31].
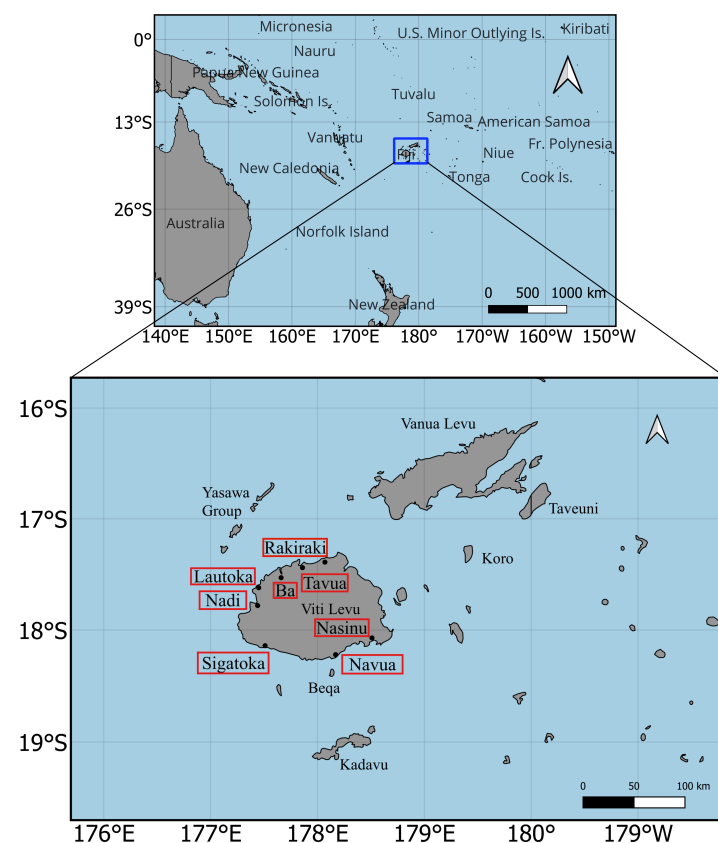

Figure 1. The geographical map shows Fiji's location in the South Pacific region and a detailed inset map highlighting various study sites within Fiji.

Fiji has a distinct dry season (May–October) and wet season (November–April). This seasonal variation is mainly attributed to the South Pacific Convergence Zone (SPCZ), the primary rainfall-producing system for the region, which lies typically over Fiji during the wet season [31,32]. The rivers and stream basins in Fiji are predominantly small in size and flow from steep mountainous terrain, resulting in rapid shifts in water levels during periods of intense rainfall, which can lead to flash floods within a few hours [33]. This study included sites only in Viti Levu due to the lack of rainfall data in other locations. These sites are areas in Fiji prone to recurrent and severe flooding events. Figure 1 shows a map of the study area and the corresponding study sites.

2.2. Dataset

The rainfall data for the Lautoka, Sigatoka, Nasinu, Rakiraki, Navua, Nadi, Ba, and Tavua sites from 1 January 2014 to 31 December 2018 (5 years) were successfully acquired from Fiji Meteorological Services. The rainfall data were provided in 5 min intervals for Tavua, Rakiraki, Nasinu, Sigatoka, and Lautoka and in 10 min intervals for the Ba, Nadi, and Navua sites. During the data pre-processing phase, the rainfall data for each site were aggregated to obtain the hourly rainfall needed for this study. If at least 66.67% of the data points (i.e., at least 4 out of 6 data points for a 10 min interval or at least 8 out of 12 data points for a 5 min interval) were available for a particular hour, they were summed to determine the total rainfall for that hour. Otherwise, the rainfall value for that hour was marked as missing. This approach was adopted to maximise the recovery of data values.

Table 1 summarises the hourly rainfall datasets and geographic settings of the study sites. The Ba site, which had a high percentage of missing values, was excluded from this study. The remaining sites had less than 5% missing values; therefore, any gap-filling method could fill in the missing values [34]. Based on the study by Oriani et al. [35], the Iterative K-nearest Neighbour (IKNN) technique was used to fill in all the missing data. The data from 1 January 2014 to 31 December 2018 were used for all the computations. However, $WRI_{24-hr-S}$ followed by $SWRI_{24-hr-S}$ were calculated from 2 January 2014 as antecedent rainfall of 24 h (the hourly rainfall data for 1 January 2014), which was necessary to allow the calculations of these metrics.

Table 1. Overview of the hourly rainfall datasets for the 8 sites in Fiji. (Note: The hourly rainfall spans from 1 January 2014 to 31 December 2018, with 43,824 expected observations.)

Study Site	Location	Missing Data (%)	Average Hourly Rainfall (mm)	Maximum Hourly Rainfall (mm)
Ba	17.53° S, 177.66° E	23.76	0.24	56.00
Lautoka	17.62° S, 177.45° E	0.83	0.19	83.50
Nadi	17.78° S, 177.44° E	1.17	0.27	260.00
Nasinu	18.07° S, 178.51° E	1.18	0.33	72.00
Navua	18.22° S, 178.17° E	1.57	0.36	62.50
Rakiraki	17.39° S, 178.07° E	3.76	0.23	68.50
Sigatoka	18.14° S, 177.51° E	1.99	0.21	59.00
Tavua	17.44° S, 177.86° E	3.45	0.16	57.50

2.3. Development of the Hourly Flood Index and Vine Copula Model

2.3.1. Hourly Flood Index and Flood Characteristics

This research formulates a novel hourly flood index ($SWRI_{24-hr-S}$), which is a normalised version of the 24-hourly water resources index ($WRI_{24-hr-S}$) proposed by Deo et al. [24]. Applying this index to Fiji is significantly advantageous because it is mathematically derived using only hourly rainfall data, which are readily available for the present study sites. The proposed $SWRI_{24-hr-S}$ is implemented using the Python programming language.

The following steps are taken to obtain the $SWRI_{24-hr-S}$. The first step is calculating the $WRI_{24-hr-S}$. The $WRI_{24-hr-S}$ for the current (i[th]) hour is given by the following equation [24]:

$$WRI^i_{24-hr-S} = P_1 + \frac{[P_2(W-1)]}{W} + \frac{[P_3(W-1-1/2)]}{W} + ... + \frac{[P_{24}(W-1-1/2-\cdots-1/23)]}{W} \qquad (1)$$

where P_1 is the total rainfall recorded an hour before, P_2 is the total rainfall recorded 2 h before, and so on; W is the time-reduction weighting factor ($W \equiv 1 + 1/2 + 1/3 + ... + 1/24 \approx 3.8$) that incorporates the contributions of accumulated rainfall in the latest 24 h [24]. This weighting factor ensures that the decay of accumulated rainfall or its potential impact on a flood event depends on several hydrological effects such as evapotranspiration, percolation, seepage, runoff, drainage, etc., in accordance with earlier works [15,24]. The substitution of $W = 3.8$ into Equation (1) yields the following:

$$WRI^i_{24-hr-S} \approx P_1 + 0.74P_2 + 0.61P_3 + ... + 0.02P_{24} \qquad (2)$$

Notably, the $WRI_{24-hr-S}$ for a current (ith) hour is expected to accumulate 100% of rainfall received an hour before, $\approx$74% of that received two hours before, $\approx$61% of that received three hours before, and eventually $\approx$2% of that received 24 h before.

After calculating $WRI_{24-hr-S}$ for any study period, the mathematical form of $SWRI_{24-hr-S}$ for a current (ith) hour is calculated as a normalised version of $WRI_{24-hr-S}$:

$$SWRI^i_{24-hr-S} = \frac{WRI^i_{24-hr-S} - \overline{WRI^{max}_{24-hr-S}}}{\sigma(WRI^{max}_{24-hr-S})} \qquad (3)$$

where $\overline{WRI^{max}_{24-hr-S}}$ is the mean monthly maximum values of $WRI_{24-hr-S}$ for the respective study period and $\sigma(WRI^{max}_{24-hr-S})$ is the standard deviation of the monthly maximum values of $WRI_{24-hr-S}$ for the respective study period.

For the purpose of this paper, we follow the notion that if the magnitude of $SWRI_{24-hr-S}$ for the current (ith) hour is greater than zero (or that the water resources are higher than normal), it is regarded as a flood situation. In this paper, we defined flood characteristics using the running-sum methodology of Yevjevich [36], which has also been used in several other studies [6,17,18]. With reference to Figure 2, the flood duration, D, is estimated as the number of hours between the start of a flood, t_{onset}, and the end of a flood, t_{end}, derived from the $SWRI_{24-hr-S}$ time series. In accordance with the onset of a flood, the volume of the flood, V, is calculated as the sum of all values of $SWRI_{24-hr-S}$ between t_{onset} and t_{end} of a flood situation, and the peak of the flood, Q, is determined as the maximum $SWRI_{24-hr-S}$ during any flood situation.
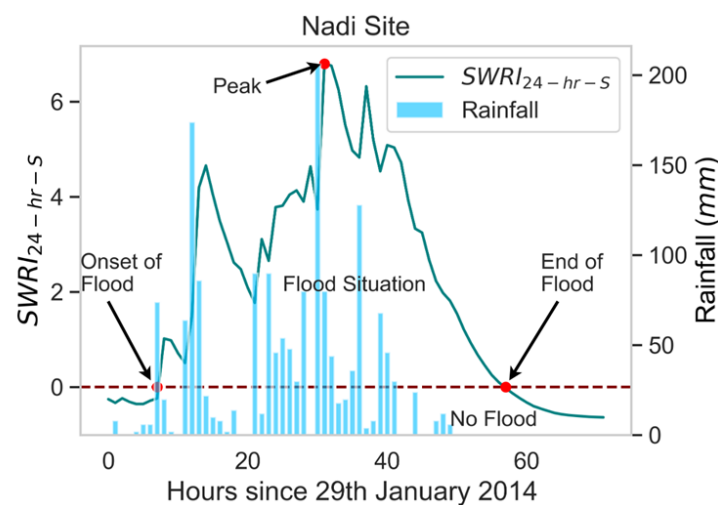

Figure 2. The $SWRI_{24-hr-S}$ developed to identify a flood event in January 2014 at the Nadi study site, demonstrating its capability to determine the duration, volume, and peak of any flood event. The flood volume, representing the accumulated water resources, is the cumulative $SWRI_{24-hr-S}$ under the curve closed by the onset and end of a flood situation and the zero line.

Equations (4)–(6) show the mathematical equations used to calculate the flood characteristics before developing the copula-probabilistic flood risk analysis model.

$$V = \sum_{t=t_{onset}}^{t=t_{end}} SWRI_{24-hr-S} \tag{4}$$

where $SWRI_{24\text{-}hr\text{-}S} > 0$

$$D = t_{end} - t_{onset} \, (hours) \tag{5}$$

$$Q = max(SWRI_{24-hr-S})_{t_{onset}-t_{end}} \tag{6}$$

where t_{onset} and t_{end} are the onset and end timestamps of a flood situation, respectively.

To demonstrate the practical use of $SWRI_{24-hr-S}$ for hourly risk flood monitoring, Figure 2 illustrates the $SWRI_{24-hr-S}$ applied to identify flood events in January 2014 at the Nadi site located in the western division of Fiji. As illustrated in Figure 2, the onset timestamp of the flood situation, i.e., the exact hour when the magnitude of $SWRI_{24-hr-S}$ starts to rise above zero, was on 29 January 2014 at 8 a.m. To verify this particular flood situation, we now refer to the report from the FMS [37], which showed indeed that an active trough that caused widespread rain across Fiji was noticeable from 29 to 30 January 2014 and resulted in flooding, particularly in the western division of Fiji, where this study site is located. Thus, this verification confirms that the proposed $SWRI_{24-hr-S}$ has correctly identified this flood event, demonstrating its practicality in identifying a flood situation at an hourly scale.

To further verify the potency of $SWRI_{24-hr-S}$ for hourly flood risk monitoring, in Figure 3, $WRI_{24-hr-S}$ is plotted alongside the hourly rainfall data for the same study site during the same period. Compared to $SWRI_{24-hr-S}$ or the raw hourly rainfall data, $SWRI_{24-hr-S}$ simplifies the process of identifying a flood situation. This is because a simple criterion, $SWRI_{24-hr-S} > 0$, provides a good indicator of flood risk, which is impossible when using $WRI_{24-hr-S}$ and the raw hourly rainfall values.
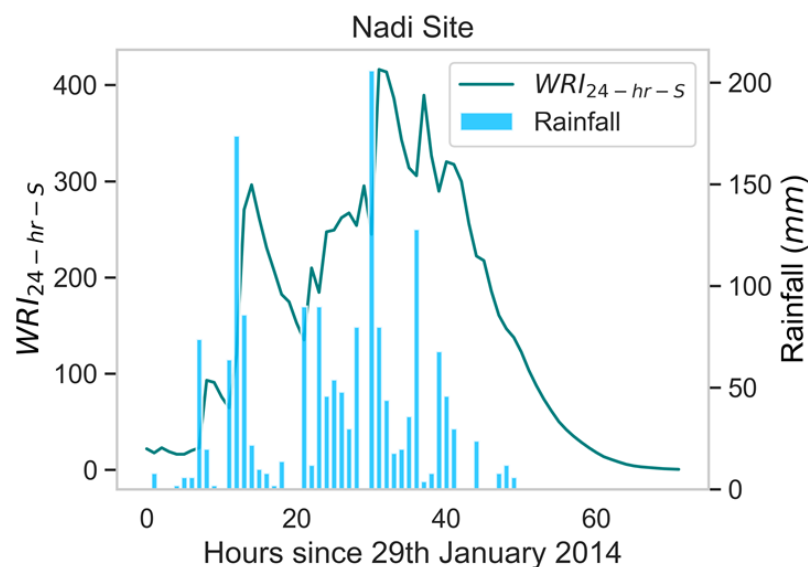

Figure 3. The $WRI_{24-hr-S}$ and rainfall since 29 January 2014 (72 h) for the Nadi site.

2.3.2. Joint Exceedance Probability between Flood Characteristics

For a comprehensive flood risk assessment, this study follows the original approach of Nguyen-Huy et al. [18] to develop vine copula-based joint exceedance probability models. This task entails developing a multivariate analysis system of flood characteristics that considers the joint exceedance probability of a flood duration D, volume V, and peak Q for the present study sites. This study specifically aimed to estimate the probability that

the duration, volume, and peak were concurrently greater than or equal to some threshold scenarios, as presented below:

$$P(D \geq d \wedge V \geq v \wedge Q \geq q) \tag{7}$$

Equation (7) requires the modelling of a joint distribution function of three variables, $F(x_d, x_v, x_q)$. Thus, in this study, we have developed a copula-based model, described in the following section, to estimate the joint exceedance probability of the flood characteristics, i.e., D, V, and Q to perform a probabilistic flood risk analysis.

2.3.3. Copula Analytical Approach

A copula $C(.) : [0,1]^n \to [0,1]$ is a function that links univariate marginal distribution functions $P(X_i \leq x_i) = F_i(x_i)$ of random variables $X_1, \ldots, X_n$ to form a joint cumulative distribution function (JCDF), $P(X_1 \leq x_1, \ldots, X_n \leq x_n) = F(x_1, \ldots, x_n)$, i.e., [26]:

$$F(x_1, \ldots, x_n) = C[F_1(x_1), \ldots, F_n(x_n)] \tag{8}$$

with the corresponding joint density distribution function (JPDF) in terms of marginal and copula probability density functions [26]:

$$f(x_1, \ldots, x_n) = \left[\prod_{i=1}^{n} f_i(x_i) \right] c[F_i(x_i), \ldots, F_n(x_n)] \tag{9}$$

where $f_i(x_i)$ and $c(.)$ are the corresponding marginal and copula PDFs, respectively. When the marginal distributions are continuous, a unique copula exists. Equations (8) and (9) demonstrate an advanced capability of copulas, allowing a JCDF of random variables to be constructed through two separate processes: (i) modelling a copula function that captures the dependence structure among correlated variables and (ii) modelling the univariate marginal distributions. This aspect of copulas presents a more flexible approach for choosing suitable univariate distribution functions to fit the observed data in practical applications. From Equation (8), the joint distribution of duration, volume, and peak given in Equation (7) can be written using copulas as follows:

$$\begin{aligned}
P(D \geq d \wedge V &\geq v \wedge Q \geq q) \\
&= 1 - F_D(d) - F_V(v) - F_Q(q) + F_{DV}(d,v) + F_{VQ}(v,q) + F_{DQ}(d,q) - F_{DVQ}(d,v,q) \\
&= 1 - F_D(d) - F_V(v) - F_Q(q) + C_{DV}[F_D(d), F_V(v)] + C_{VQ}[F_V(v), F_Q(q)] + \\
&\qquad C_{DQ}[F_D(d), F_Q(q)] - C_{DVQ}[F_D(d), F_V(v), F_Q(q)]
\end{aligned} \tag{10}$$

Different copula families, such as empirical, Archimedean, extreme value, elliptical, vine, and entropy copulas, can be used to model the copula function given in Equation (10) [38,39]. Vine copulas, among other copulas, can be used to achieve the utmost flexibility in constructing the JCDF and JPDF, given in Equations (8) and (9), respectively. Vine copulas have been applied in recent studies across various fields, such as weather and climate risk in agriculture [40,41], hydrology and water resources [27,42–48], and finance and insurance [49–51]. The following section provides more details on vine copulas.

2.3.4. Vine Copulas

The vine copula was first introduced by Joe [52], whose concept was to decompose the JPDF into a cascade of iteratively conditioned bivariate copulas, also called pair copulas. While this decomposition is not unique, all possible decompositions can be organised into a graphical model called a regular vine (R-vine) [53].

Within the R-vine framework, two main types of vine copula decomposition exist: the canonical (C-vine) and drawable (D-vine) distributions. These modes determine the parametric construction of an R-vine. The D-vine copula offers higher flexibility than

the C-vine copula, especially when considering all mutual inter-correlations between targeted random variables one after another [47]. However, the C- and D-vine frameworks are the same when considering a 3-dimensional (3D) (or tri-variate) joint distribution framework [18,47].

In this study, we have focused on tri-variate cases to model the joint distribution of flood duration, volume, and peak for a detailed probabilistic risk analysis of any flood event. Figure 4 shows a graphical representation of D- and C-vine copulas in the form of trees, edges, and nodes.
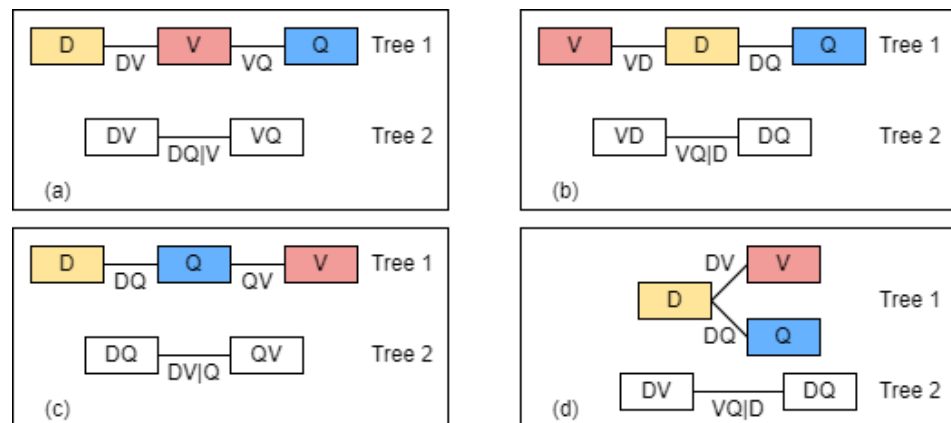

Figure 4. Schematic diagram of different ways of constructing the 3D D-vine copula structure in this study. (**a**) Case 1: the flood volume (V) as a conditioning variable, (**b**) Case 2: the flood duration (D) as a conditioning variable, (**c**) Case 3: the flood peak (Q) as a conditioning variable, and (**d**) an example of the C-vine copula structure. Source: Adapted from Nguyen-Huy et al. [18].

In the tri-variate case where D, V, and Q are modelled simultaneously, the C-vine copula is the D-vine copula with a specified centre variable, as previously mentioned. For instance, when the flood duration (D) variable serves as the centre variable, the D-vine copula depicted in Figure 4b is identical to the C-vine copula shown in Figure 4d. The edges are linked to bivariate copulas, such as the edge DV associated with the bivariate copula C_{DV}, which captures the dependence structure between D and V.

To fit the univariate marginal distribution functions, we employed the univariate local-polynomial likelihood kernel density estimation method capable of handling discrete (duration) and continuous (volume and peak) data [54]. Additionally, the following bivariate copula families were utilised to develop the 3D vine copula models in this study: independence, parametric (elliptical, Archimedean, and their rotated versions), and non-parametric (transformation kernel) families [54–56] (Table A1).

To estimate the parameters of bivariate copulas, we employed maximum likelihood for parametric models and local-likelihood approximations for non-parametric models. Moreover, the modified vine copula Bayesian information criteria (mBICv) [57] was utilised to select the bivariate copulas, and Kendall's tau (τ) was adopted to select tree sequences [18]. The mBICv can address the issues of the Bayesian information criterion (BIC), which assumes that the number of possible parameters grows sufficiently slowly with the sample size n and that all models are equally likely. Additionally, the mBICv was explicitly tailored to vine copula models [57]. The vine copula models were developed using the R programming language utilising the 'rvinecopulib' library package [54].

3. Results and Discussion

We now provide a detailed appraisal of the hourly flood index $SWRI_{24-hr-S}$ for detecting hourly flood possibility in terms of the onset and the end timestamps, duration, peak, volume, and total accumulated rainfall during any flood situation for seven study sites in Fiji over the study period (2014–2018). We also provide joint distribution model

results using the newly proposed vine copulas to provide a probabilistic risk analysis framework for flash floods.

3.1. Application of the Hourly Flood Index for Flood Event Analysis

The $WRI_{24-hr-S}$, followed by the $SWRI_{24-hr-S}$ for the study period (2014–2018), were successfully computed for each of the seven study sites. The practicality of $SWRI_{24-hr-S}$ for determining a flood situation has already been demonstrated in Figure 2. Similarly, the flood events between 3 and 6 April 2016 were quantified. This was first done for the Tavua site as it was one of the severely flooding-impacted areas in the western division of Fiji [58].

Our analysis identified four flood events using the criterion $SWRI_{24-hr-S} > 0$ to indicate a flood situation (Figure 5) for the Tavua site. Of four flood events, the two significant events were predominantly caused by heavy rain in the past 24 h. The first major flood event started on 3 April at 5 p.m. and ended on 4 April at 4 p.m. with a total duration of 23 h, a volume of 20.37, and a peak of 2.36. Approximately 154 mm of rainfall was recorded during this event. The second major flood event started on the 6th of April at 3 a.m. and lasted for 14 h. This flood event recorded a total volume of 8.77, with a peak of 1.03, while approximately 69.50 mm of rainfall was recorded for this event. The combined volume of all four flood events for the Tavua site between 3 April 2016 and 6 April 2016 (96 h) was 30.59.
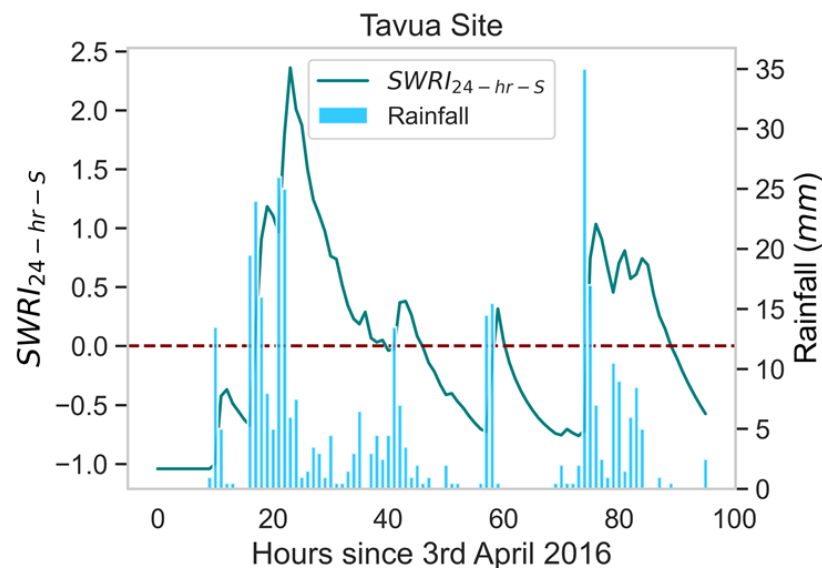

Figure 5. The $SWRI_{24-hr-S}$ applied to identify the flood events in April 2016 at the Tavua site (96 h).

The flood events for the same period were also determined for the other six sites. The flood characteristics, i.e., *D*, *V*, and *Q* of the floods, varied among these sites, as shown in Figure 6. The results showed that areas in the western division of Fiji were severely affected by flooding, as was reported by FMS [58] [Tavua ($V \approx 30.59$), Lautoka ($V \approx 25.63$), Sigatoka ($V \approx 19.45$), Nadi ($V \approx 9.12$), and Rakiraki ($V \approx 8.79$)] compared to the areas in the central division [Navua ($V \approx 0.12$) (minor flood event), and Nasinu (no floods)]. These results demonstrate the utility of $SWRI_{24-hr-S}$ in identifying flood situations and determining their characteristics. Consequently, the proposed $SWRI_{24-hr-S}$ can be considered a feasible and cost-effective tool to monitor the flash flood risk in Fiji. The variation in flood characteristics among our study sites demonstrates the importance of flood risk assessments for each site separately, despite the proximity of these sites, as also highlighted in previous work [6]. Figure 7 depicts the occurrence of floods, encompassing minor events with minimal volume and potentially insignificant impacts at each of the seven study sites over 2014–2018. Over this five-year study period, a slight fluctuation in flood frequency was observed across the study sites, as illustrated in Figure 7. Notably, the Tavua study site

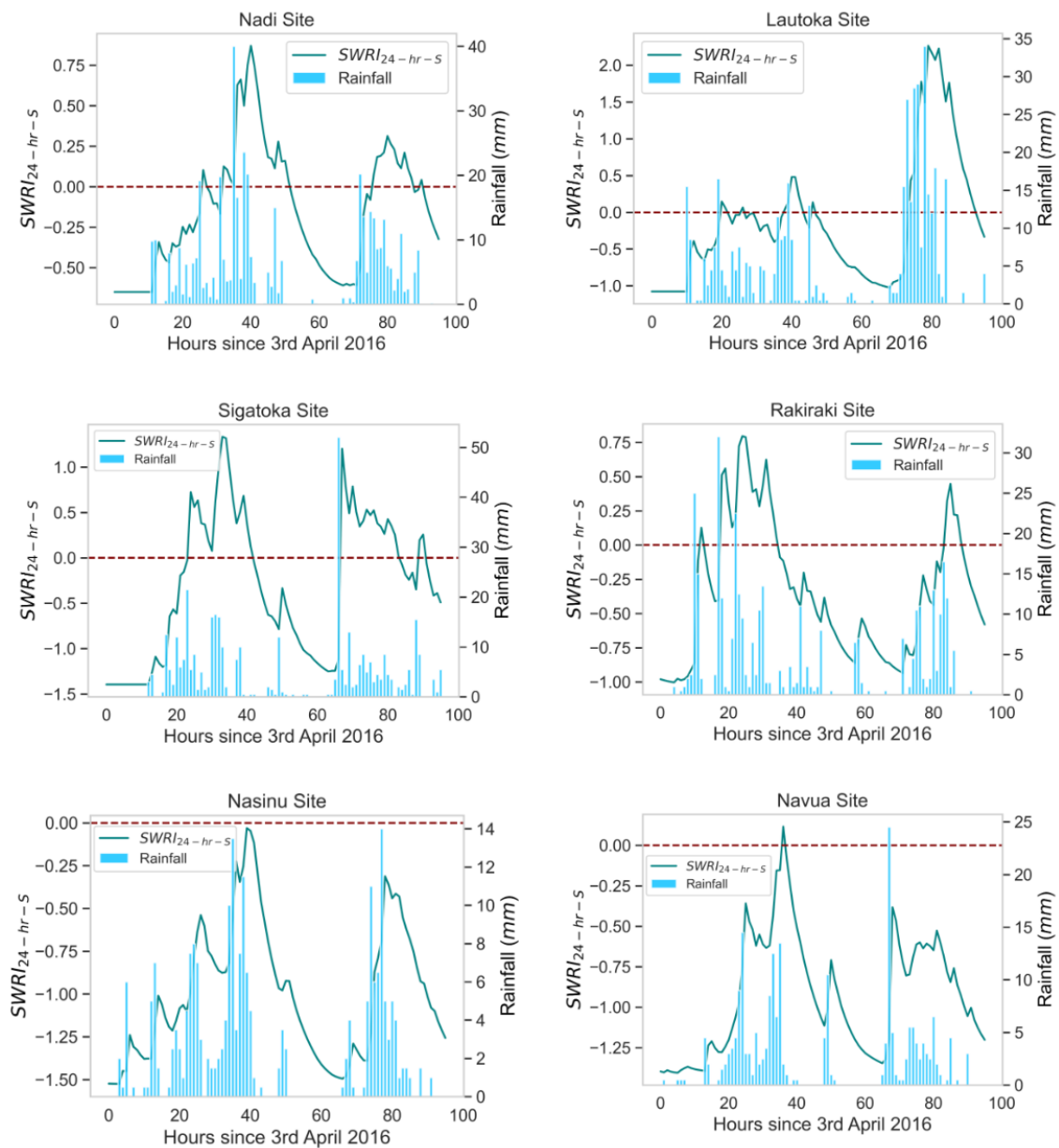exhibited the highest frequency, while the Nasinu study site recorded the lowest frequency of flood events.

Figure 6. The $SWRI_{24-hr-S}$ applied to identify the flood events in April 2016 at the other study sites (96 h).

The occurrence of frequent severe weather events, such as tropical cyclones and depressions, results in significant flood events in Fiji, and this usually occurs during the wet season (November–April) and occasionally in the dry season (May–October), especially in La Niña years [33]. This is evident in Figure 8, which indicates the wet season, including May and October, experiencing high rainfall, leading to a higher frequency of flood events and greater flood volume (Figure 9) compared to the other months. This emphasises the need for Fiji's National Disaster Management Office (NDMO) and other relevant stakeholders to implement comprehensive flood mitigation and resilience measures. Public education on flood safety and preparedness for the wet season is also crucial, particularly for those residing in flood-prone areas.
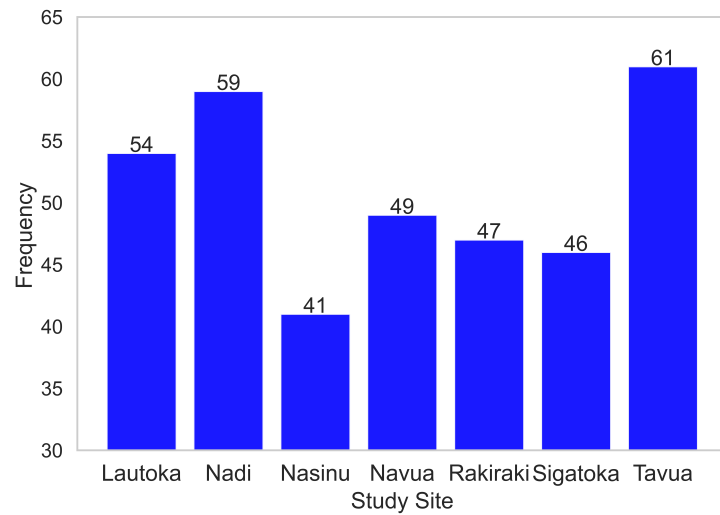
Figure 7. Geographic analysis of flood frequency between 2014 and 2018.
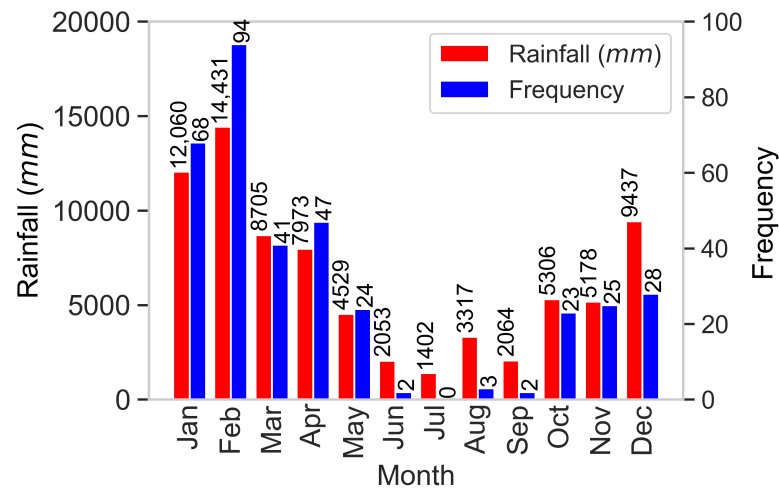

Figure 8. Temporal (monthly) analysis of flood frequency and total monthly rainfall aggregated from 2014 to 2018.
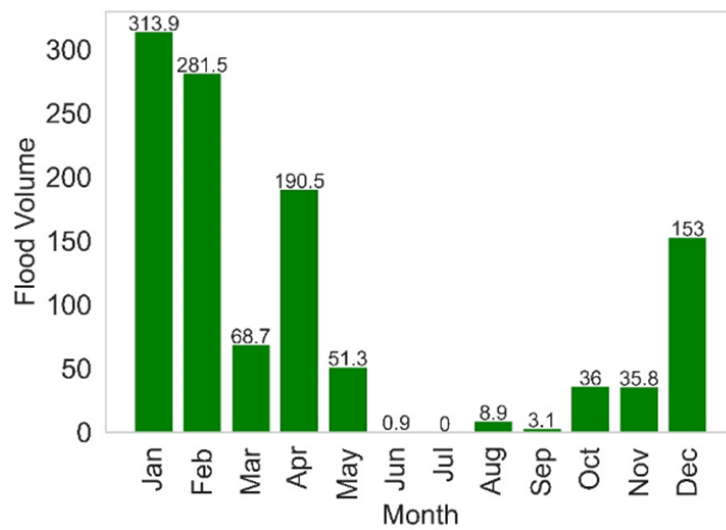

Figure 9. Temporal (monthly) analysis of the combined volume of flood events across 7 study sites from 2014 to 2018.

The annual rainfall and the occurrence of flood events across seven sites from 2014 to 2018 are illustrated in Figure 10. This figure shows that the year 2015 had the lowest rainfall among all years examined. According to FMS [59], the rainfall trends in 2015 exhibited a typical El Niño pattern, characterised by below-average rainfall at most of the study stations. Consequently, there were fewer flood events (Figure 10) and a lower flood volume (Figure 11) in 2015 compared to the other years in the present study.
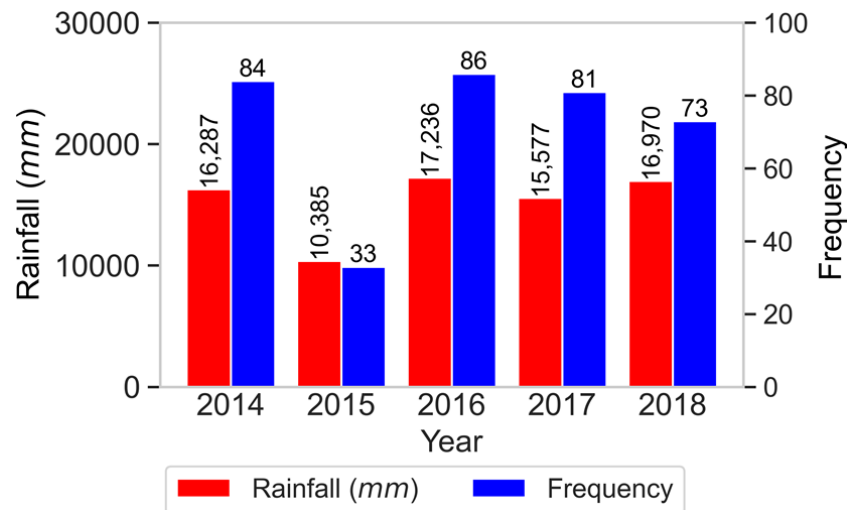

Figure 10. Frequency of floods and total rainfall across 7 study sites aggregated from 2014 to 2018.
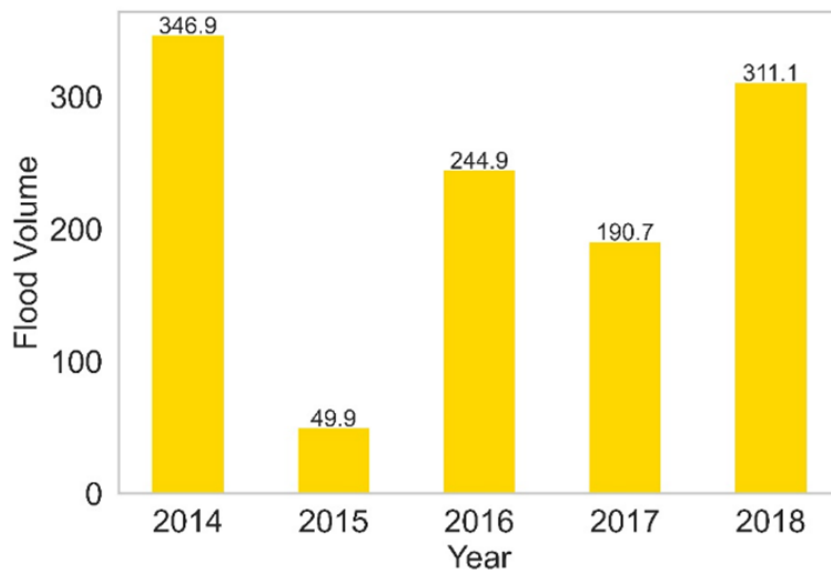
Figure 11. Yearly combined volume of flood events across 7 study sites from 2014 to 2018.

Table 2 lists the five severe floods at each of the seven sites during the study period. The flood severity was determined by ranking the flood events at each site based on their volume, with 1 indicating the most severe and 5 indicating the least severe. For each of the seven sites, the table displays the onset time, duration, volume, peak, total $WRI_{24-hr-S}$, total rain, and maximum $WRI_{24-hr-S}$ for each flood event. Statistics such as these may aid relevant organisations in understanding past flood events at these sites, which will facilitate future flood mitigation decisions to minimise the severity of floods at these locations.

A brief analysis of the most severe flood event at each study site was performed and validated using the annual climate summaries published by the Fiji Meteorological Services to ensure that the $SWRI_{24-hr-S}$ accurately identified them. The analysis of floods in Nadi (Table 2a) showed that the most severe flood started on 29 January 2014 at 8 a.m. and

recorded a volume of 157.28. This flood lasted 49 h and reached a peak of 6.80, making it the most severe flood event with the most prolonged duration among all the study sites during the 5-year study period. During this flood event, about 1590 mm of rainfall was recorded. This flood event was described in Figure 2 and validated using Fiji's annual climate summary for 2014 [37].

Table 2b shows that the most severe flood event in Lautoka recorded a total volume of 25.05. This flood event started on 14 January 2018 at 2 p.m. and lasted 19 h, reaching a peak of 3.29. During this flood event, about 175 mm of rainfall was recorded. This flood event was verified using Fiji's climate summaries 2018, which stated that heavy rainfall occurred from 13 to 15 January 2018 due to an active trough of low pressure, resulting in widespread flooding [60,61].

Table 2. Analysis of the 5 most severe flood events for different study sites in Fiji from 2014 to 2018. (**a**) Nadi, (**b**) Lautoka, (**c**) Nasinu, (**d**) Navua, (**e**) Rakiraki, (**f**) Sigatoka, and (**g**) Tavua.

Study Site		Onset Time (t_{onset})	Volume (V)	Duration (D) (hrs)	Peak (Q)	Total $WRI_{24-hr-S}$	Total Rain (mm)	Maximum $WRI_{24-hr-S}$
a	Nadi							
	1	29 January 2014 at 8 a.m.	157.28	49	6.80	10,557.06	1590	416.05
	2	8 February 2017 at 4 a.m.	11.88	18	1.31	1316.32	195.40	109.56
	3	4 April 2016 at 8 a.m.	6.86	20	0.87	1108.52	161.40	84.87
	4	7 January 2014 at 6 p.m.	6.31	10	1.73	715.09	84	133.10
	5	15 January 2014 at 6 p.m.	5.77	13	1.18	794.02	84	102.03
b	Lautoka							
	1	14 January 2018 at 2 p.m.	25.05	19	3.29	1315.15	175	126.10
	2	6 April 2016 at 2 a.m.	23.95	19	2.27	1283.34	180	96.59
	3	1 April 2014 at 7 a.m.	18.39	13	3.49	935.98	109	131.92
	4	6 February 2017 at 3 p.m.	11.48	20	1.53	954.55	131.50	75.40
	5	8 February 2017 at 9 a.m.	10.85	13	1.49	718.16	98	74.18
c	Nasinu							
	1	27 February 2014 at 9 a.m.	24.90	18	2.83	1388.83	173	115.53
	2	21 February 2015 at 6 p.m.	23.15	16	2.48	1261.37	163.50	106.16
	3	6 December 2014 at 4 a.m.	19.15	16	2.92	1155.37	140	117.79
	4	11 November 2018 at 11 p.m.	7.46	8	1.91	521.64	37	91.16
	5	28 May 2018 at 8 a.m.	7.20	7	2.10	474.23	21	96.15
d	Navua							
	1	15 December 2016 at 6 a.m.	56.98	28	4.29	2732.99	392.50	161.35
	2	17 March 2017 at 4 a.m.	16.37	14	2.10	1023.68	114.50	99.48
	3	16 January 2014 at 1 a.m.	9.82	14	1.16	838.28	123.50	72.87
	4	2 May 2016 at 6 a.m.	8.15	13	1.38	751.01	110	79.03
	5	27 February 2014 at 3 p.m.	7.98	10	1.61	626.25	83.50	85.60
e	Rakiraki							
	1	19 December 2016 at 5 a.m.	33.99	21	4.28	1783.89	265.50	170.39
	2	14 January 2018 at 2 p.m.	19.89	17	2	1199.35	156.50	97.02
	3	20 February 2016 at 8 p.m.	16.89	17	2.68	1103.01	112.50	119.05
	4	17 December 2016 at 4 p.m.	11.28	19	1.25	989.33	145.50	73.09
	5	5 March 2017 at 9 a.m.	10.06	15	1.52	818.03	114.50	81.73
f	Sigatoka							
	1	30 January 2014 at 10 a.m.	23.32	16	2.84	999.93	121	92.83
	2	3 February 2018 at 3 p.m.	15	12	2.25	695.39	93	79.78
	3	1 May 2018 at 6 p.m.	11.10	14	1.67	671.12	65	67.25
	4	4 April 2016 at 12 a.m.	10.91	18	1.33	789.16	103	59.79
	5	1 April 2018 at 6 a.m.	9.74	11	1.55	549.66	73	64.62
g	Tavua							
	1	8 February 2017 at 10 a.m.	45.88	23	4.04	1612.79	238	117.34
	2	3 April 2016 at 5 p.m.	20.37	23	2.36	1023.74	154	78.55
	3	17 May 2014 at 10 a.m.	17.16	17	1.81	805.30	103.50	65.93
	4	6 February 2017 at 11 a.m.	14.77	18	1.69	774.08	89.50	63.11
	5	6 March 2017 at 1 p.m.	14.23	17	1.75	737.52	98.50	64.47

According to Table 2c, the most severe flood in Nasinu started on 27 February 2014 at 9 a.m. and lasted 18 h. This flood had a volume of 24.90 and reached a peak of 2.83.

Approximately 173 mm of rainfall was recorded during this flood event. As reported by FMS [37], the tropical depressions TD14F and TD15F caused heavy rainfall in Fiji's central and eastern divisions between 25 and 27 February 2014. As a result, parts of Fiji, particularly the major river systems in the central division (where this study site is located), experienced flooding during this period.

The most severe flood, both in Navua (Table 2d) and Rakiraki (Table 2e), occurred in December 2016. For Navua, this event started on 15 December 2016 at 6 a.m. and lasted for 28 h, during which it recorded a volume of 56.98 and reached a peak of 4.29. For Rakiraki, it started on the 19th of December at 5 a.m. and lasted for 21 h, during which it recorded a volume of 33.99 and reached a peak of 4.28. Approximately 392.50 mm and 265.50 mm of rainfall were recorded during this flood event for Navua and Rakiraki, respectively. The most severe flood event that occurred at the Navua and Rakiraki sites was validated using Fiji's climate summaries 2016, which stated that the trough of low pressure and active rain bands associated with the tropical depression TD04F resulted in heavy rainfall that caused severe flooding in some parts of the country's main island of Viti Levu (where these study sites are located) from 12 to 20 December 2016 [58].

Based on Table 2f, the most severe flood event in Sigatoka started on 30 January 2014 at 10 a.m. and lasted for 16 h. This flood had a volume of 23.32 and reached a peak of 2.84. Approximately 121 mm of rainfall was recorded during this flood event. As mentioned earlier, an active trough that caused widespread rain across Fiji from the 29 to the 30 January 2014 resulted in flooding, particularly in the western division of Fiji, where this site is located [37].

Lastly, the analysis of floods in Tavua (Table 2g) showed that the most severe flood started on 8 February 2017 at 10 a.m. and recorded a volume of 45.88. This flood lasted 23 h and reached a peak of 4.04. During this flood event, about 238 mm of rainfall was recorded. As per FMS [62], the tropical depression TD09F affected the country between 6 and 8 February 2017 and led to flooding in parts of the western division of Fiji, where this study site is located.

3.2. Application of the Vine Copula Model for Probabilistic Flood Risk Analysis

The frequency of flood events at each study site is demonstrated in Figure 7. Similarly, the flood characteristics, i.e., D, V, and Q, for each flood event were calculated for all study sites. Table 3 shows the five-number summary, including the mean, standard deviation, skewness, and kurtosis for each flood characteristic at each study site.

Moreover, as shown in Table 3, the minimum flood duration was 1 h at all study sites. The maximum flood duration, volume, and peak were recorded at the Nadi site (this flood event is described in Figure 2). The skewness and kurtosis information of each flood characteristic, which describes the shape and distribution of a dataset, were more than +1 and +3, respectively, for all study sites, indicating that their distribution is highly right-skewed. This means the flood characteristics dataset for all study sites contains extreme flood duration, volume, and peak values.

The results in Table 3 also show that flood characteristics exhibit high variability across all study sites in terms of their median and inter-quartile range (IQR). The median flood duration for all study sites was 3 h, while the median volume and peak ranged from approximately 0.52 to 0.89 and 0.24 to 0.42, respectively. The IQR for flood duration, volume, and peak varied from 4 to 7 h, 1.78 to 2.94, and 0.52 to 0.91, respectively. The high spatiotemporal variation in flood characteristics highlights the importance of modelling these characteristics simultaneously, and employing a robust model like the copulas used in this study is crucial for accurately capturing the dependence among these flood characteristics.

Table 3. Descriptive statistics of flood characteristics at each study site.

Flood Characteristic	Site	Min.	Lower Quartile (Q1)	Median (Q2)	Upper Quartile (Q3)	Max.	Mean	Standard Dev.	Skewness	Kurtosis
Duration (D) (hours)	Lautoka	1	1	3	6	20	4.796	4.791	1.771	5.511
	Nadi	1	1	3	7	49	5.424	7.135	4.286	24.981
	Rakiraki	1	1	3	8	21	5.681	5.801	1.248	3.243
	Tavua	1	2	3	7	23	5.525	5.749	1.590	4.492
	Sigatoka	1	1	3	5	18	4.413	4.578	1.746	4.848
	Navua	1	1	3	5	28	4.367	5.003	2.753	11.676
	Nasinu	1	2	3	6	18	4.415	4.153	1.962	6.236
Volume (V)	Lautoka	0.003	0.204	0.633	1.983	25	2.746	5.473	3.022	11.168
	Nadi	0.002	0.132	0.517	2.271	157.276	4.156	20.404	7.538	55.625
	Rakiraki	0.005	0.097	0.529	3.038	33.993	3.272	6.329	3.257	13.998
	Tavua	0.016	0.185	0.617	2.272	45.879	3.190	7.123	4.230	22.984
	Sigatoka	0.021	0.220	0.632	2.834	23.316	2.826	4.777	2.523	9.293
	Navua	0.005	0.167	0.557	2.058	56.983	3.012	8.495	5.656	34.803
	Nasinu	0.033	0.159	0.886	2.854	24.903	3.028	5.853	2.951	10.098
Peak (Q)	Lautoka	0.003	0.179	0.348	0.701	3.490	0.597	0.725	2.519	9.356
	Nadi	0.002	0.108	0.244	0.674	6.803	0.527	0.940	5.369	35.042
	Rakiraki	0.005	0.097	0.323	0.816	4.282	0.606	0.809	2.663	10.954
	Tavua	0.016	0.124	0.338	0.799	4.040	0.573	0.688	2.719	12.339
	Sigatoka	0.021	0.207	0.393	1.121	2.841	0.718	0.714	1.369	3.945
	Navua	0.005	0.167	0.401	0.723	4.289	0.601	0.747	2.924	13.398
	Nasinu	0.033	0.139	0.419	0.916	2.915	0.720	0.763	1.566	4.596

Conducting a comprehensive correlation analysis among flood characteristics and understanding the relationship between each characteristic pair is another crucial step in modelling their joint distribution [18]. In this study, both parametric measures—Pearson's correlation coefficient (r)—and nonparametric rank-based correlation measures—Spearman's correlation coefficient (ρ) and Kendall's tau (τ)—were employed to examine the relationship between each pair of flood characteristics. Additionally, Mutual Information (MI) was utilised to examine the degree of dependence between each pair of flood characteristics. The results obtained are presented in Table 4. The correlation coefficients, i.e., r, ρ, and τ, obtained between each pair of flood characteristics, were statistically significant at the 1% level of significance. Overall, a strong positive dependency is observed between each pair of flood characteristics across all study sites, as shown in Table 4. However, there would be cases where the peak value is extremely high while the duration is low or the peak is moderate while the duration is long, and the volumes would also be different. For example, as shown in Table 4, at the Tavua site, the linear correlation measured by Pearson's correlation coefficient between D and Q ($r_{D\&Q} \approx 0.859$) is higher than that between D and V ($r_{D\&Q} \approx 0.838$). However, the rank correlation measured by Spearman's and Kendall's tau correlation coefficients between D and Q ($\rho_{D\&Q} \approx 0.902, \tau_{D\&Q} \approx 0.698$) are lower than those between D and V ($\tau_{D\&V} \approx 0.946, \tau_{D\&V} \approx 0.836$). This implies complex and non-linear relationships among flood characteristics. Subsequently, the risks of different flood events are different. Therefore, this requires a robust model like copulas used in this study to capture the full dependence among flood characteristics.

Additionally, it must be noted that across all study sites, the strongest dependencies exist between $D - V$ and $V - Q$ compared to $D - Q$. This is particularly evident based on Kendall's tau (τ) coefficient utilised in this study to select the most optimal structure of the vine copula model at each study site. This implies that the flood volume, V, can be positioned between the other two flood characteristics (i.e., D and Q), as illustrated in Figure 4a, to model the joint distribution of D, V, and Q using the 3D D-vine copula.

Table 4. The statistical correlation in terms of the Pearson's correlation coefficient (r), Spearman's rank correlation coefficient (ρ), Kendall's tau (τ), and Mutual Information (MI) computed between the pairs of flood characteristics, i.e., Duration (D, in hours), Volume (V), and Peak (Q) for each study site.

Site	D&V				D&Q				V&Q			
	r	ρ	τ	*MI*	*r*	ρ	τ	*MI*	*r*	ρ	τ	*MI*
Lautoka	0.895	0.941	0.831	1.051	0.860	0.877	0.738	0.584	0.931	0.971	0.883	1.044
Nadi	0.863	0.950	0.849	0.966	0.929	0.891	0.740	0.619	0.924	0.978	0.890	0.771
Rakiraki	0.855	0.934	0.828	0.823	0.842	0.902	0.760	0.647	0.949	0.987	0.926	1.123
Sigatoka	0.895	0.929	0.820	0.851	0.810	0.869	0.721	0.616	0.887	0.979	0.888	1.129
Tavua	0.838	0.946	0.836	0.983	0.859	0.902	0.698	0.651	0.942	0.960	0.859	1.103
Navua	0.891	0.937	0.838	1.066	0.937	0.892	0.752	0.616	0.899	0.982	0.903	0.933
Nasinu	0.942	0.945	0.831	0.903	0.895	0.844	0.687	0.501	0.896	0.964	0.844	0.904

Table 5 shows the results obtained when the 3D D-vine copula is fitted to the flood characteristics data at each study site. As depicted in Table 5, the results confirm that the D-vine structure illustrated in Figure 4a with flood volume (V) as the conditioning variable is the most appropriate to model the joint distribution of flood characteristics (i.e., D, V, and Q) across all study sites. The table also shows the best-fitted bivariate copula function and its associated parameters at each tree level for each study site. For instance, at the Sigatoka site, in the first tree (Tree 1), the Frank (C_{DV}) and Survival Gumbel (C_{VQ}) copulas are selected between $D - V$ and $V - Q$, respectively. In the second tree (Tree 2), the Frank copula is chosen as the most parsimonious for identifying the bivariate copula ($C_{DQ|V}$).

Table 5. Overall summary of fitted 3D D-vine copula framework at each study site. Note: τ = Kendall's tau, logLik = Log-Likelihood, AIC = Akaike Information Criterion, and BIC = Bayesian Information Criterion.

Site	D-Vine Structure (Conditioning Variable)	Tree Level	Flood Characteristic Pairs	Best-Fitted Copula	Copula Dependence Parameter (s)	τ	logLik	AIC	BIC
Lautoka		Tree 1	D-V	Gaussian	$\rho = 0.93$	0.77	102.58	−199.16	−193.19
			V-Q	Gaussian	$\rho = 0.94$	0.78			
		Tree 2	DQ│V	Gumbel	$\theta = 1.1$	0.08			
Nadi		Tree 1	D-V	Frank	$\theta = 15$	0.77	142.45	−278.89	−272.66
			V-Q	BB7	$\theta = 2.1$; $\delta = 11.6$	0.81			
		Tree 2	DQ│V	Independence	NA	0			
Nasinu		Tree 1	D-V	Gaussian	$\rho = 0.93$	0.75	72.98	−141.96	−138.53
			V-Q	Gaussian	$\rho = 0.92$	0.75			
		Tree 2	DQ│V	Independence	NA	0			
Navua	D-V-Q (V is placed in the centre)	Tree 1	D-V	Frank	$\theta = 16$	0.78	111.65	−219.29	−215.51
			V-Q	Survival Gumbel (Rotated Gumbel 180 degrees)	$\theta = 6.4$	0.84			
		Tree 2	DQ│V	Independence	NA	0			
Rakiraki		Tree 1	D-V	Gaussian	$\rho = 0.93$	0.75	118.13	−230.25	−224.70
			V-Q	BB7	$\theta = 3$; $\delta = 15$	0.83			
		Tree 2	DQ│V	Independence	NA	0			
Sigatoka		Tree 1	D-V	Frank	$\theta = 20$	0.82	123.88	−241.76	−236.27
			V-Q	Survival Gumbel (Rotated Gumbel 180 degrees)	$\theta = 7$	0.86			
		Tree 2	DQ│V	Frank	$\theta = -3.6$	−0.36			
Tavua		Tree 1	D-V	Survival BB7 (Rotated BB7 180 degrees)	$\theta = 5.2$; $\delta = 3.6$	0.77	148.44	−288.87	−280.43
			V-Q	BB7	$\theta = 4.3$; $\delta = 13.4$	0.82			
		Tree 2	DQ│V	Independence	NA	0			

To derive the joint exceedance probability of the flood event characteristics (i.e., D, V, and Q) for different combination scenarios using the best-fitted 3D D-vine copula selected at each study site, we first quantify the probability that the flood duration, volume, and peak exceed specific thresholds simultaneously (Equation (7)). The thresholds were selected at the 50th quantile (median), 75th quantile (moderate), and 95th quantile (extreme). The quantile values of each flood characteristic were computed and subsequently averaged for all study sites, as presented in Table 6. As seen in Table 6, for example, the averaged 50th-quantile value of duration is $q_D(0.5) = 3$ h. Similarly, the averaged 75th-quantile value of duration is $q_D(0.75) = 6$ h, and the averaged 95th-quantile value of duration is $q_D(0.95) = 15$ h. As for the spatial pattern, Table 6 demonstrates a moderate variation in the quantile values of each flood characteristic across all study sites.

Table 6. The duration (D) (hours), volume (V), and peak (Q) at the 50th quantile (median), 75th quantile (moderate), and 95th quantile (extreme) for each study site.

Flood Characteristic	Study Site	50th Quantile	75th Quantile	95th Quantile
D (hours)	Lautoka	3	6	15
	Nadi	3	7	13
	Rakiraki	3	8	17
	Tavua	3	7	17
	Sigatoka	3	5	16
	Navua	3	5	14
	Nasinu	3	6	16
	Average	3	6	15
V	Lautoka	0.633	1.983	13.898
	Nadi	0.517	2.271	6.365
	Rakiraki	0.529	3.038	15.205
	Tavua	0.617	2.272	14.767
	Sigatoka	0.632	2.834	11.054
	Navua	0.557	2.058	9.149
	Nasinu	0.866	2.854	19.153
	Average	0.622	2.473	12.799
Q	Lautoka	0.348	0.701	1.840
	Nadi	0.244	0.674	1.365
	Rakiraki	0.323	0.816	1.976
	Tavua	0.338	0.799	1.750
	Sigatoka	0.393	1.121	2.305
	Navua	0.401	0.723	1.694
	Nasinu	0.419	0.916	2.477
	Average	0.352	0.821	1.915

By applying the vine copula probabilistic model, we show the joint exceedance probabilities of the duration, volume, and peak in different combination scenarios for each study site in Figures 12–14. From a flood risk analysis perspective, the present results clearly demonstrate a moderate yet notable difference in spatial patterns of the joint exceedance probability of flood event characteristics in different combination scenarios. As shown in Figure 12a, the probabilities of a flood event occurring where both the volume and peak exceed the 50th-quantile (median) values (i.e., $V \geq q(0.50) = 0.622$ and $Q \geq q(0.50) = 0.352$) and the duration (D) exceeds the median (i.e., $D \geq q(0.50) = 3$ h), moderate (i.e., $D \geq q(0.75) = 6$ h), and extreme (i.e., $D \geq q(0.95) = 15$ h) values are approximately 50–59%, 23–39%, and 4–10% across all study sites, respectively.
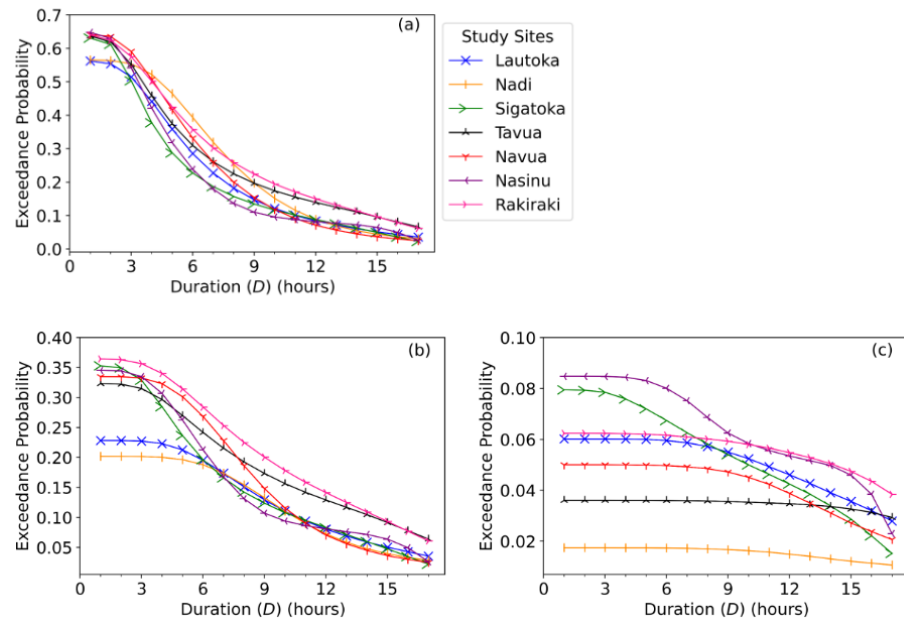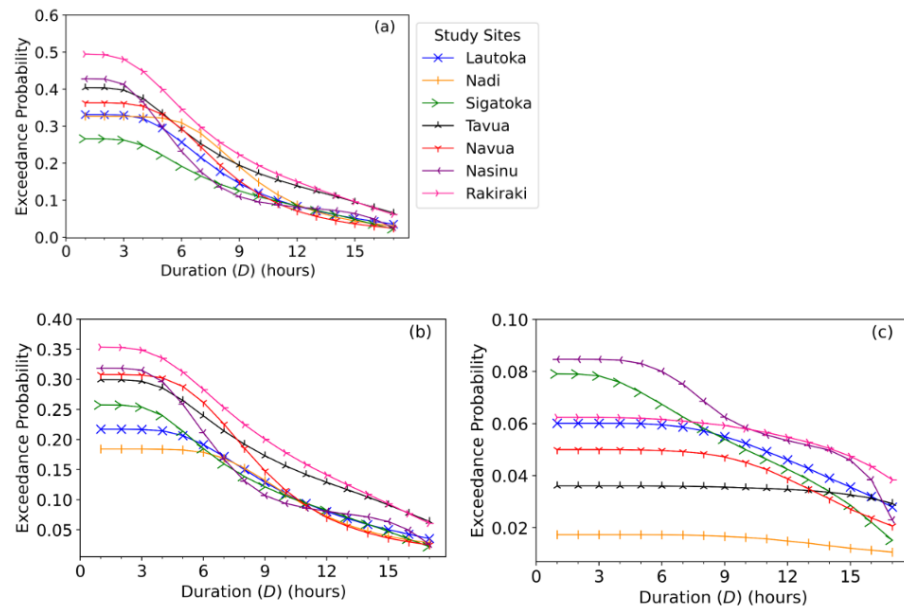
Figure 12. Flood risk assessment presented in terms of the joint exceedance probability of a flood event's duration (*D*) being greater than or equal to the 50th quantile (median) (i.e., $D \geq q$ (0.5) = 3 h), 75th quantile (moderate) (i.e., $D \geq q$ (0.75) = 6 h), and 95th quantile (extreme) (i.e., $D \geq q$ (0.95) = 15 h) combined with the following: (**a**) both the volume and peak being greater than or equal to the 50th quantile (i.e., $V \geq q$ (0.5) = 6.222 & $Q \geq q$ (0.5) = 0.352)), (**b**) the volume being greater than or equal to the 50th quantile and the peak being greater than or equal to the 75th quantile (i.e., $V \geq q$ (0.5) = 6.222 & $Q \geq q$ (0.75) = 0.821), and (**c**) the volume being greater than or equal to the 50th quantile and the peak being greater than or equal to the 95th quantile (i.e., $V \geq$ q (0.5) = 6.222 & $Q \geq q$ (0.95) = 1.915).
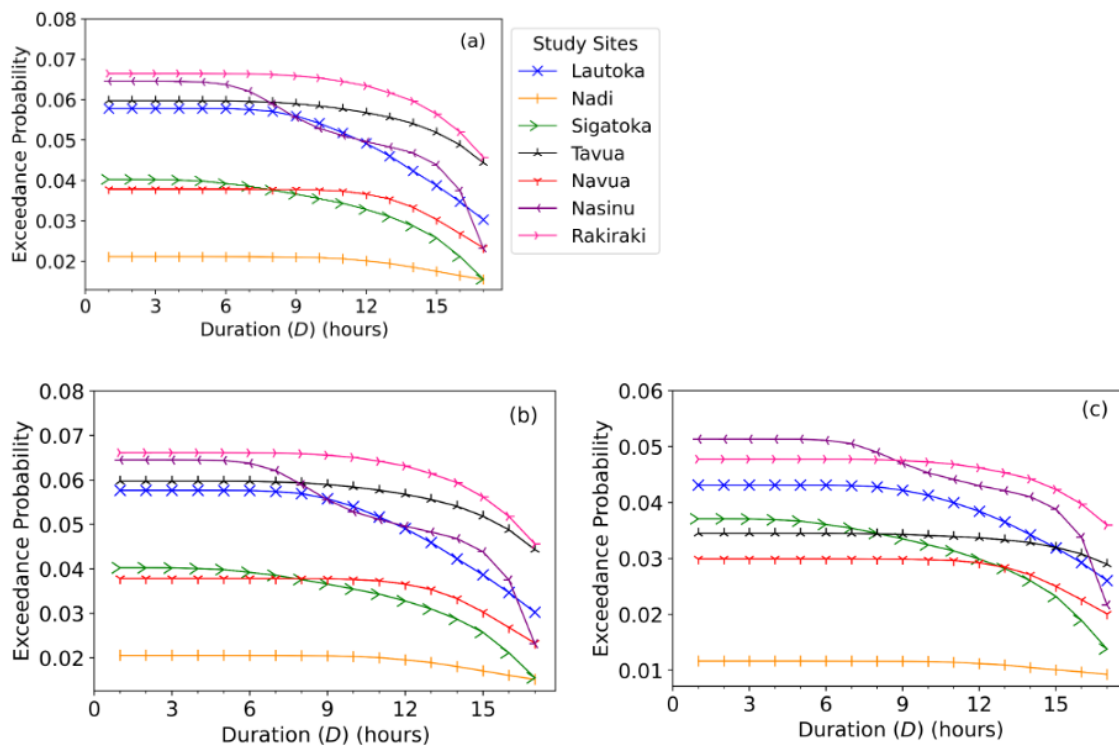

Figure 13. Flood risk assessment presented in terms of the joint exceedance probability of the flood duration (*D*) being greater than or equal to the 50th quantile (median) (i.e., $D \geq q$ (0.5) = 3 h), 75th quantile (moderate) (i.e., $D \geq q$ (0.75) = 6 h), and 95th quantile (extreme) (i.e., $D \geq q$ (0.95) = 15 h) combined with the following: (**a**) the volume being greater than or equal to the 75th quantile and the peak being greater than or equal to the 50th quantile (i.e., $V \geq q$ (0.75) = 2.473 & $Q \geq q$ (0.5) = 0.352), (**b**) both the volume and peak being greater than or equal to the 75th quantile (i.e., $V \geq q$ (0.75) = 2.473 & $Q \geq q$ (0.75) = 0.821), and (**c**) the volume being greater than or equal to the 75th quantile and the peak being greater than or equal to the 95th quantile (i.e., $V \geq q$ (0.75) = 2.473 & $Q \geq q$ (0.95) = 1.915).

Figure 14. Flood risk assessment presented in terms of the joint exceedance probability of the flood duration (D) being greater than or equal to the 50th quantile (median) (i.e., $D \geq q$ (0.5) = 3 h), 75th quantile (moderate) (i.e., $D \geq q$ (0.75) = 6 h), and 95th quantile (extreme) (i.e., $D \geq q$ (0.95) = 15 h) combined with the following: (**a**) the volume being greater than or equal to the 95th quantile and the peak being greater than or equal to the 50th quantile (i.e., $V \geq q$ (0.95) = 12.799 & $Q \geq q$ (0.5) = 0.352), (**b**) the volume being greater than or equal to the 95th quantile and the peak being greater than or equal to the 75th quantile (i.e., $V \geq q$ (0.95) = 12.799 & $Q \geq q$ (0.75) = 0.821), and (**c**) both the volume and peak being greater than or equal to the 95th quantile (i.e., $V \geq q$ (0.95) = 12.799 & $Q \geq q$ (0.95) = 1.915).

A similar probabilistic flood risk analysis conducted with both the volume and peak exceeding the 75th-quantile (moderate) values (i.e., $V \geq q$ (0.75) = 2.473 and $Q \geq q$ (0.75) = 0.821) and the duration (D) exceeding the median (i.e., $D \geq q$ (0.50) = 3 h), moderate (i.e., $D \geq q$ (0.75) = 6 h), and extreme (i.e., $D \geq q$ (0.95) = 15 h) values showed that the probability of flood occurrence was approximately 18–35%, 18–28%, and 4–9% across all study sites, respectively (Figure 13b).

In general, the probability of a flood event with a volume exceeding the 50th-quantile (median) or 75th-quantile (moderate) values and both the peak and duration exceeding the 95th-quantile (extreme) value was less than 5% across all study sites. In the case when both the flood volume and duration exceeded the 95th-quantile (extreme) value, the probability of a flood event with the peak exceeding the 50th-quantile (median) or 75th-quantile (moderate) values was less than 6% across all study sites.

In the worst-case scenario, when the flood risk could be more severe, we found that the probability of a flood event occurring where the volume, peak, and duration exceeded the extreme values (i.e., $V \geq q$ (0.95) = 12.799, $Q \geq q$ (0.95) = 1.915, and $D \geq q$ (0.95) = 15 h) was less than 5% at all study sites (Figure 14c). These findings imply a moderate probability of a flood event characterised by median (i.e., 50th-quantile) duration, volume, and peak values across all study sites. The results also suggest that the likelihood of a flood event characterised by extreme duration, volume, and peak is exceptionally low across all study sites.

4. Conclusions, Limitations of the Study and Future Research Directions

This study has made novel contributions to flood risk monitoring and assessment by developing a mathematically convenient hourly flood index, $SWRI_{24-hr-S}$, and testing its practical use in identifying flood situations over 2014-2018 at seven different study sites in Fiji while jointly modelling flood characteristics such as flood duration, volume, and peak using a vine copula model for probabilistic flood risk assessment.

The results have unambiguously established the practical use of the newly proposed $SWRI_{24-hr-S}$ as a potent indicator to identify the flood situation at an hourly scale while computing the associated flood characteristics that were impossible with a 24-hourly water resources index used in the literature. The results also showed that Fiji mainly experienced high rainfall during the wet/cyclone season (November to April), including May and October. Consequently, the number of flood events was higher in these months than in the other months. This highlights the critical importance of implementing comprehensive and well-structured flood preparedness and risk mitigation strategies tailored explicitly for these months characterised by increased rainfall and flood events, thus ensuring the safety and security of communities and their properties. This study also presented the flood characteristics and water-intensive properties of five severe flood events for each study site. Relevant organisations, such as Fiji's NDMO, are expected to use these findings to understand the attributes of past flood events at these study sites. This, in turn, can support future decision-making on flood mitigation, ultimately reducing the severe impacts of such events.

The results also demonstrated a strong positive dependency between each pair of flood characteristics across all study sites. The D-vine structure with flood volume (V) as the conditioning variable was identified as the most appropriate for modelling the joint distribution of flood characteristics (i.e., D, V, and Q) across all study sites. Therefore, it was utilised to model the joint distributions among the extreme flood characteristics to extract their joint exceedance probability, providing crucial information for probabilistic flood risk assessment at each study site. The findings revealed moderate variations in the spatial patterns of joint exceedance probability of extreme flood event characteristics across different combination scenarios, underscoring exceptionally low probabilities of floods with extreme duration, volume, and peak at all study sites.

Despite the merits of the present study, a primary limitation of this research was the unavailability of rainfall data required for many of the flood-prone sites across Fiji. Consequently, this research was confined to selected sites within the western and central divisions of the country. As a result, this study could not perform a comparative analysis across all four divisions (i.e., the western, central, northern, and eastern divisions), which could have provided valuable insights into extreme flood risk areas in the nation. It is important to note that the Ba study site in the western division of Fiji, a frequent flooding zone, had to be excluded due to a high percentage of missing rainfall data. Therefore, in future research, our methodology can be improved with $SWRI_{24-hr-S}$ derived from satellite-based rainfall products covering a wider area, including major towns and cities, following the recent approach for Myanmar [18].

Another limitation of the present study was using a prior/fixed time-dependent reduction function with the weighting factor, $W = 3.8$, derived in an earlier study [24] to determine the contributions of accumulated rainfall in the latest 24 h. As discussed, the proposed $SWRI_{24-hr-S}$ is a normalised version of an existing $WRI_{24-hr-S}$ that used a suitable time-dependent reduction function to account for the depletion of water resources through various hydrological processes. It must be noted that the results of this study are sensitive to the value of W. A change in W will alter the contributions of accumulated rainfall in the latest 24 h in Equation (2). Consequently, both $WRI_{24-hr-S}$ and the proposed $SWRI_{24-hr-S}$ will change accordingly.

In the future, further studies can test the correctness of this weighting factor (W) more comprehensively for study sites where the topography may vary considerably. This could require a major correlation of this weighting factor against rainfall-runoff and other

physical models to capture more accurately the actual value of the decay of accumulated rainfall and its impacts on a flood event [15,24]. Several tests with hydrological parameters, including evapotranspiration rates, percolation, seepage, surface runoff, and drainage conditions, etc., may be required to ascertain the time-dependent reduction function for $SWRI_{24-hr-S}$. In regions with different decay rates of rainfall-accumulated water volume, it is crucial to incorporate them when formulating $SWRI_{24-hr-S}$. The proposed $SWRI_{24-hr-S}$ must also be verified for its broader adoption as an index-based risk monitoring tool. Therefore, its feasibility is expected to be demonstrated in other flood-prone regions globally in future studies, contingent on the availability of well-documented flood records for validation and hourly rainfall data. While doing so, a different technique to normalise the existing $WRI_{24-hr-S}$ may be selected, depending on how the normalised $WRI_{24-hr-S}$ index represents flood risk situations in those climatic conditions.

This study has undertaken a purely mathematical-based approach to monitoring flood risk, so in future studies, it is anticipated that the proposed $SWRI_{24-hr-S}$, in conjunction with additional data such as the catchment hydrology, drainage information, and river flows, will be utilised to develop hourly hydrographs for various sites. This approach will further cement the accuracy of flood characteristic estimation and the monitoring of flash flood events. There is also the potential to develop an innovative $SWRI_{24-hr-S}$-based forecasting system with sufficient lead time, presenting a novel approach for early flash flood warnings in Fiji and other regions.

A key advantage of $SWRI_{24-hr-S}$, as an hourly flood risk monitoring tool, is its simplistic mathematical formula that is easy to compute, analyse, and interpret for non-expert audiences compared to physical or hydrological models, including rainfall-runoff models for flood risk monitoring that involves complex development. However, in the future, especially in varied hydrological and topographic settings, it is crucial to comprehensively compare the proposed $SWRI_{24-hr-S}$ with other established flood monitoring systems, including the Flash Flood Guidance System (FFGS).

Despite these limitations, using $SWRI_{24-hr-S}$ has demonstrated acceptable accuracy in detecting flood situations on an hourly scale. Therefore, our proposed methodology can be considered a feasible and cost-effective tool for hourly flood risk monitoring in Fiji and perhaps other similar geographical locations. Applying the proposed probabilistic flood risk analysis using vine copulas can enhance the nation's overall flood risk assessment and mitigation strategies.

Abbreviations

The following abbreviations are used in this manuscript:

AIC	Akaike Information Criterion
API	Antecedent Precipitation Index
AWRI	Available Water Resources Index
BIC	Bayesian Information Criterion
D	Flood Duration
FFGS	Flash Flood Guidance System
FJD	Fijian Dollar
FMS	Fiji Meteorological Services
GDP	Gross Domestic Product
I_F	Daily Flood Index
IQR	Interquartile Range
JCDF	Joint Cumulative Distribution Function
JPDF	Joint Density Distribution Function
logLik	Log-Likelihood
mBICv	Modified Vine Copula Bayesian Information Criteria
NDMO	Fiji's National Disaster Management Office
PDF	Probability Density Function
PSIDS	Pacific Small Island Developing State
Q	Flood Peak
r	Pearson's Correlation Coefficient
SAPI	Standardised Antecedent Precipitation Index
SPCZ	South Pacific Convergence Zone
SPI	Standardised Precipitation Index
SWAP	Standardised Weighted Average of Precipitation
$SWRI_{24-hr-S}$	Hourly Flood Index
USD	United States Dollar
V	Flood Volume
WAP	Weighted Average of Precipitation
$WRI_{24-hr-S}$	24-Hourly Water Resources Index
ρ	Spearman's Rank Correlation Coefficient
τ	Kendall's Tau Correlation Coefficient

Appendix A

Table A1. The bivariate copula families utilised to develop the 3D D-vine copula models in this study.

Copula Type	Bivariate Copula Family	Name
	Elliptical	Gaussian
		Student-t
Parametric	Archimedean	Frank
		Gumble
		Rotated Gumbel 90 degrees
		Rotated Gumbel 180 degrees (Survival Gumbel)
		Rotated Gumbel 270 degrees
		Clayton
		Rotated Clayton 90 degrees
		Rotated Clayton 180 degrees (Survival Clayton)
		Rotated Clayton 270 degrees
		Joe
		Rotated Joe 90 degrees
		Rotated Joe 180 degrees (Survival Joe)
		Rotated Joe 270 degrees

Table A1. *Cont.*

Copula Type	Bivariate Copula Family	Name
		Clayton-Gumbel (BB1)
		Rotated BB1 90 degrees
		Rotated BB1 180 degrees (Survival BB1)
		Rotated BB1 270 degrees
		Joe-Gumbel (BB6)
		Rotated BB6 90 degrees
		Rotated BB6 180 degrees (Survival BB6)
		Rotated BB6 270 degrees
		Joe- Clayton (BB7)
		Rotated BB7 90 degrees
		Rotated BB7 180 degrees (Survival BB7)
		Rotated BB7 270 degrees
		Joe-Frank (BB8)
		Rotated BB8 90 degrees
		Rotated BB8 180 degrees (Survival BB8)
		Rotated BB8 270 degrees
Non-parametric	-	Transformation kernel
-	-	Independence

References

1. Taherizadeh, M.; Khushemehr, J.H.; Niknam, A.; Nguyen-Huy, T.; Mezősi, G. Revealing the effect of an industrial flash flood on vegetation area: A case study of Khusheh Mehr in Maragheh-Bonab Plain, Iran. *Remote Sens. Appl. Soc. Environ.* **2023**, *32*, 101016. [CrossRef]
2. Taherizadeh, M.; Niknam, A.; Nguyen-Huy, T.; Mezősi, G.; Sarli, R. Flash flood-risk areas zoning using integration of decision-making trial and evaluation laboratory, GIS-based analytic network process and satellite-derived information. *Nat. Hazards* **2023**, *118*, 2309–2335. [CrossRef]
3. Associated Programme on Flood Management. Management of Flash Floods. Integrated Flood Management Tools Series No. 16, World Meteorological Organization. 2012. Available online: https://www.floodmanagement.info/publications/tools/APFM_Tool_16.pdf (accessed on 11 January 2024).
4. Shah, V.; Kirsch, K.R.; Cervantes, D.; Zane, D.F.; Haywood, T.; Horney, J.A. Flash flood swift water rescues, Texas, 2005–2014. *Clim. Risk Manag.* **2017**, *17*, 11–20. [CrossRef]
5. Dordevic, M.; Mutic, P.; Kim, H. Flash Flood Guidance System: Response to One of the Deadliest Hazards. WMO Bulletin 1, World Meteorological Organization. 2020. Available online: https://www.imgw.pl/sites/default/files/2020-04/wmo_klimat_woda_en-min.pdf (accessed on 11 January 2024).
6. Moishin, M.; Deo, R.C.; Prasad, R.; Raj, N.; Abdulla, S. Development of Flood Monitoring Index for daily flood risk evaluation: Case studies in Fiji. *Stoch. Environ. Res. Risk Assess.* **2021**, *35*, 1387–1402. [CrossRef]
7. Sharma, K.K.; Verdon-Kidd, D.C.; Magee, A.D. A decision tree approach to identify predictors of extreme rainfall events–a case study for the Fiji Islands. *Weather Clim. Extrem.* **2021**, *34*, 100405. [CrossRef]
8. Davis, J.; Henion, D.; Murro, M.J. *The Impacts of Coastal Flooding on Physical Infrastructure: Case Studies in Fiji, Kiribati, and Papua New Guinea*; Report; Center for Excellence in Disaster Management & Humanitarian Assistance: Ford Island, HI, USA , 2022.
9. Government of Fiji. Climate Vulnerability Assessment: Making Fiji Climate Resilient. Report, Government of Fiji. 2017. Available online: https://reliefweb.int/report/fiji/climate-vulnerability-assessment-making-fiji-climate-resilient (accessed on 11 January 2024).
10. The World Bank Group. Data. 2024. Available online: https://data.worldbank.org/country/fiji?view=chart (accessed on 11 January 2024).
11. Leonard, M.; Westra, S.; Phatak, A.; Lambert, M.; van den Hurk, B.; McInnes, K.; Risbey, J.; Schuster, S.; Jakob, D.; Stafford-Smith, M. A compound event framework for understanding extreme impacts. *Wiley Interdiscip. Rev. Clim. Change* **2014**, *5*, 113–128. [CrossRef]
12. Seneviratne, S.I.; Nicholls, N.; Easterling, D.; Goodess, C.M.; Kanae, S.; Kossin, J.; Luo, Y.; Marengo, J.; McInnes, K.; Rahimi, M.R.; et al. Changes in Climate Extremes and their Impacts on the Natural Physical Environment. In *Managing the Risks of Extreme Events and Disasters to Advance Climate Change Adaptation: Special Report of the Intergovernmental Panel on Climate Change*; Field, C.B., Barros, V., Stocker, T.F., Dahe, Q., Dokken, D.J., Ebi, K.L., Mastrandrea, M.D., Mach, K.J., Plattner, G.K., Allen, S.K., et al., Eds.; Cambridge University Press: Cambridge, UK; New York, NY, USA, 2012; pp. 109–230. [CrossRef]

13. Seiler, R.; Hayes, M.; Bressan, L. Using the standardized precipitation index for flood risk monitoring. *Int. J. Climatol. J. R. Meteorol. Soc.* **2002**, *22*, 1365–1376. [CrossRef]

14. Byun, H.R.; Lee, D.K. Defining three rainy seasons and the hydrological summer monsoon in Korea using available water resources index. *J. Meteorol. Soc. Jpn.* **2002**, *80*, 33–44. [CrossRef]

15. Lu, E. Determining the start, duration, and strength of flood and drought with daily precipitation: Rationale. *Geophys. Res. Lett.* **2009**, *36*, L12707. [CrossRef]

16. Lu, E.; Cai, W.; Jiang, Z.; Zhang, Q.; Zhang, C.; Higgins, R.W.; Halpert, M.S. The day-to-day monitoring of the 2011 severe drought in China. *Clim. Dyn.* **2014**, *43*, 1–9. [CrossRef]

17. Deo, R.C.; Byun, H.R.; Adamowski, J.F.; Kim, D.W. A real-time flood monitoring index based on daily effective precipitation and its application to Brisbane and Lockyer Valley flood events. *Water Resour. Manag.* **2015**, *29*, 4075–4093. [CrossRef]

18. Nguyen-Huy, T.; Kath, J.; Nagler, T.; Khaung, Y.; Aung, T.S.S.; Mushtaq, S.; Marcussen, T.; Stone, R. A satellite-based Standardized Antecedent Precipitation Index (SAPI) for mapping extreme rainfall risk in Myanmar. *Remote Sens. Appl. Soc. Environ.* **2022**, *26*, 100733. [CrossRef]

19. Nguyen-Huy, T.; Deo, R.C.; Yaseen, Z.M.; Prasad, R.; Mushtaq, S. Bayesian Markov chain Monte Carlo-based copulas: Factoring the role of large-scale climate indices in monthly flood prediction. In *Intelligent Data Analytics for Decision-Support Systems in Hazard Mitigation: Theory and Practice of Hazard Mitigation*; Deo, R.C., Kisi, O., Samui, P., Yaseen, Z.M., Eds.; Springer Nature: Singapore, 2021; pp. 29–47. [CrossRef]

20. Prasad, R.; Charan, D.; Joseph, L.; Nguyen-Huy, T.; Deo, R.C.; Singh, S. Daily flood forecasts with intelligent data analytic models: Multivariate empirical mode decomposition-based modeling methods. In *Intelligent Data Analytics for Decision-Support Systems in Hazard Mitigation: Theory and Practice of Hazard Mitigation*; Deo, R.C., Kisi, O., Samui, P., Yaseen, Z.M., Eds.; Springer Nature: Singapore, 2021; pp. 359–381. [CrossRef]

21. Nosrati, K.; Saravi, M.M.; Shahbazi, A. Investigation of flood event possibility over Iran using Flood Index. In *Survival and Sustainability: Environmental Concerns in the 21st Century*; Gökçekus, H., Türker, U., LaMoreaux, J.W., Eds.; Environmental Earth Sciences; Springer: Berlin/Heidelberg, Germany, 2011; pp. 1355–1361.

22. Deo, R.C.; Adamowski, J.F.; Begum, K.; Salcedo-Sanz, S.; Kim, D.W.; Dayal, K.S.; Byun, H.R. Quantifying flood events in Bangladesh with a daily-step flood monitoring index based on the concept of daily effective precipitation. *Theor. Appl. Climatol.* **2019**, *137*, 1201–1215. [CrossRef]

23. Ahmed, A.M.; Farheen, S.; Nguyen-Huy, T.; Raj, N.; Jui, S.J.J.; Farzana, S. Real-time prediction of the week-ahead flood index using hybrid deep learning algorithms with synoptic climate mode indices. *Res. Sq.* **2023**. [CrossRef]

24. Deo, R.C.; Byun, H.R.; Kim, G.B.; Adamowski, J.F. A real-time hourly water index for flood risk monitoring: Pilot studies in Brisbane, Australia, and Dobong Observatory, South Korea. *Environ. Monit. Assess.* **2018**, *190*, 1–27. [CrossRef]

25. Chebana, F.; Ouarda, T.B. Index flood–based multivariate regional frequency analysis. *Water Resour. Res.* **2009**, *45*, W10435. [CrossRef]

26. Sklar, M. Fonctions de répartition à n dimensions et leurs marges. *Ann. l'ISUP* **1959**, *8*, 229–231.

27. Daneshkhah, A.; Remesan, R.; Chatrabgoun, O.; Holman, I.P. Probabilistic modeling of flood characterizations with parametric and minimum information pair-copula model. *J. Hydrol.* **2016**, *540*, 469–487. [CrossRef]

28. Shafaei, M.; Fakheri-Fard, A.; Dinpashoh, Y.; Mirabbasi, R.; De Michele, C. Modeling flood event characteristics using D-vine structures. *Theor. Appl. Climatol.* **2017**, *130*, 713–724. [CrossRef]

29. Tosunoglu, F.; Gürbüz, F.; İspirli, M.N. Multivariate modeling of flood characteristics using Vine copulas. *Environ. Earth Sci.* **2020**, *79*, 1–21. [CrossRef]

30. Kuleshov, Y.; McGree, S.; Jones, D.; Charles, A.; Cottrill, A.; Prakash, B.; Atalifo, T.; Nihmei, S.; Seuseu, F.L.S.K. Extreme weather and climate events and their impacts on island countries in the Western Pacific: Cyclones, floods and droughts. *Atmos. Clim. Sci.* **2014**, *4*, 803. [CrossRef]

31. Feresi, J.; Kenny, G.J.; de Wet, N.; Limalevu, L.; Bhusan, J.; Ratukalou, I. *Climate Change Vulnerability and Adaptation Assessment for Fiji*; Technical Report; The International Global Change Institute (IGCI), University of Waikato: Hamilton, New Zealand, 2000.

32. Kumar, R.; Stephens, M.; Weir, T. Rainfall trends in Fiji. *Int. J. Climatol.* **2014**, *34*, 1501–1510. [CrossRef]

33. McGree, S.; Yeo, S.W.; Devi, S. *Flooding in the Fiji Islands between 1840 and 2009*; Risk Frontiers Technical Report, Risk Frontiers; Macquarie University: Macquarie Park, Australia, 2010.

34. Lo Presti, R.; Barca, E.; Passarella, G. A methodology for treating missing data applied to daily rainfall data in the Candelaro River Basin (Italy). *Environ. Monit. Assess.* **2010**, *160*, 1–22. [CrossRef]

35. Oriani, F.; Stisen, S.; Demirel, M.C.; Mariethoz, G. Missing data imputation for multisite rainfall networks: A comparison between geostatistical interpolation and pattern-based estimation on different terrain types. *J. Hydrometeor.* **2020**, *21*, 2325–2341. [CrossRef]

36. Yevjevich, V.M. Objective Approach to Definitions and Investigations of Continental Hydrologic Droughts. Ph.D. Thesis, Colorado State University, Fort Collins, CO, USA, 1967.

37. FMS. Fiji Annual Climate Summary 2014. Report, Fiji Meteorological Service. 2015. Available online: https://www.met.gov.fj/aifs_prods/ACS-2014.pdf (accessed on 11 January 2024).

38. Nguyen-Huy, T.; Deo, R.C.; Mushtaq, S.; Kath, J.; Khan, S. Copula-based agricultural conditional value-at-risk modelling for geographical diversifications in wheat farming portfolio management. *Weather Clim. Extrem.* **2018**, *21*, 76–89. [CrossRef]

39. Nguyen-Huy, T.; Deo, R.C.; Khan, S.; Devi, A.; Adeyinka, A.A.; Apan, A.A.; Yaseen, Z.M. Student performance predictions for advanced engineering mathematics course with new multivariate copula models. *IEEE Access* **2022**, *10*, 45112–45136. [CrossRef]
40. Nguyen-Huy, T.; Deo, R.C.; Mushtaq, S.; Kath, J.; Khan, S. Copula statistical models for analyzing stochastic dependencies of systemic drought risk and potential adaptation strategies. *Stoch. Environ. Res. Risk Assess.* **2019**, *33*, 779–799. [CrossRef]
41. Nguyen-Huy, T.; Kath, J.; Mushtaq, S.; Cobon, D.; Stone, G.; Stone, R. Integrating El Niño-Southern Oscillation information and spatial diversification to minimize risk and maximize profit for Australian grazing enterprises. *Agron. Sustain. Dev.* **2020**, *40*, 4. [CrossRef]
42. Ni, L.; Wang, D.; Wu, J.; Wang, Y.; Tao, Y.; Zhang, J.; Liu, J.; Xie, F. Vine copula selection using mutual information for hydrological dependence modeling. *Environ. Res.* **2020**, *186*, 109604. [CrossRef]
43. Nguyen-Huy, T.; Deo, R.C.; Mushtaq, S.; Khan, S. Probabilistic seasonal rainfall forecasts using semiparametric d-vine copula-based quantile regression. In *Handbook of Probabilistic Models*; Samui, P., Chakraborty, S., Bui, D.T., Deo, R.C., Eds.; Elsevier: Oxford, UK, 2020; pp. 203–227. [CrossRef]
44. Cheng, Y.; Du, J.; Ji, H. Multivariate joint probability function of earthquake ground motion prediction equations based on vine copula approach. *Math. Probl. Eng.* **2020**, *2020*, 1697352. [CrossRef]
45. Lü, T.J.; Tang, X.S.; Li, D.Q.; Qi, X.H. Modeling multivariate distribution of multiple soil parameters using vine copula model. *Comput. Geotech.* **2020**, *118*, 103340. [CrossRef]
46. Latif, S.; Mustafa, F. Parametric vine copula construction for flood analysis for Kelantan river basin in Malaysia. *Civ. Eng. J.* **2020**, *6*, 1470–1491. [CrossRef]
47. Latif, S.; Simonovic, S.P. Parametric Vine copula framework in the trivariate probability analysis of compound flooding events. *Water* **2022**, *14*, 2214. [CrossRef]
48. Latif, S.; Simonovic, S.P. Trivariate Joint Distribution Modelling of Compound Events Using the Nonparametric D-Vine Copula Developed Based on a Bernstein and Beta Kernel Copula Density Framework. *Hydrology* **2022**, *9*, 221. [CrossRef]
49. Czado, C.; Bax, K.; Sahin, Ö.; Nagler, T.; Min, A.; Paterlini, S. Vine copula based dependence modeling in sustainable finance. *J. Financ. Data Sci.* **2022**, *8*, 309–330. [CrossRef]
50. Jeong, H.; Dey, D. Application of a vine copula for multi-line insurance reserving. *Risks* **2020**, *8*, 111. [CrossRef]
51. Allen, D.E.; McAleer, M.; Singh, A.K. Risk measurement and risk modelling using applications of vine copulas. *Sustainability* **2017**, *9*, 1762. [CrossRef]
52. Joe, H. *Multivariate Models and Multivariate Dependence Concepts*; Chapman & Hall/CRC: Boca Raton, FL, USA, 1997.
53. Nagler, T.; Krüger, D.; Min, A. Stationary vine copula models for multivariate time series. *J. Econom.* **2022**, *227*, 305–324. [CrossRef]
54. Nagler, T.; Vatter, T. Rvinecopulib: High Performance Algorithms for Vine Copula Modeling. R Package Version 3, CRAN. 2023. Available online: https://cran.r-project.org/web/packages/rvinecopulib/rvinecopulib.pdf (accessed on 11 January 2024).
55. Nagler, T.; Czado, C. Evading the curse of dimensionality in nonparametric density estimation with simplified vine copulas. *J. Multivar. Anal.* **2016**, *151*, 69–89. [CrossRef]
56. Nagler, T.; Schellhase, C.; Czado, C. Nonparametric estimation of simplified vine copula models: Comparison of methods. *Depend. Model.* **2017**, *5*, 99–120. [CrossRef]
57. Nagler, T.; Bumann, C.; Czado, C. Model selection in sparse high-dimensional vine copula models with an application to portfolio risk. *J. Multivar. Anal.* **2019**, *172*, 180–192. [CrossRef]
58. FMS. Fiji Annual Climate Summary 2016. Report, Fiji Meteorological Service. 2017. Available online: https://www.met.gov.fj/Summary2.pdf (accessed on 11 January 2024).
59. FMS. Fiji Annual Climate Summary 2015. Report, Fiji Meteorological Service. 2016. Available online: https://www.met.gov.fj/aifs_prods/ACS-2015.pdf (accessed on 11 January 2024).
60. FMS. Fiji's Climate in 2018. Report, Fiji Meteorological Service. 2019. Available online: https://www.met.gov.fj/aifs_prods/Climate_Products/December (accessed on 11 January 2024).
61. FMS. Fiji Climate Summary January 2018. Report, Fiji Meteorological Service. 2018. Available online: https://www.met.gov.fj/aifs_prods/FSCJAN18.pdf (accessed on 11 January 2024).
62. FMS. Fiji Annual Climate Summary 2017. Report, Fiji Meteorological Service. 2018. Available online: https://www.met.gov.fj/aifs_prods/Climate_Products/2017annualSum2020.01.28 (accessed on 11 January 2024).